Heat and Mass Transfer (2023) 59:1707–1747
https://doi.org/10.1007/s00231-023-03358-8

REVIEW

A critical review on recent developments and applications of microchannels in the field of heat transfer and energy

Achintya Kambli[1] · **Prasenjit Dey**[1]

Received: 2 November 2022 / Accepted: 13 March 2023 / Published online: 18 April 2023

Abstract
There is a rapid movement towards miniaturization in the field of micro-electronics, medical, defence, and space applications as well as an increase in thermal load density in the field of solar power. This has resulted in the requirement for technologies to be developed which enable the rapid removal of high thermal load from the components for effective and safe operation. Microchannel cooling has been one of the areas which has been investigated to provide the solution as required. This paper aims to looks at the different types of microchannels being developed, review the performance of microchannels being developed with different working fluids, explore the various structures utilized of microchannels and explore the use of microchannel in the various applications with regards to field of thermal management. Finally, future needs are proposed for extending the research and enlarging its application fields. This review paper serves as guidance for researchers to design and predict the performance of microchannel heat sinks (MCHS).

1 Introduction

In the recent times there is a growing push towards miniaturization in the field of electronics. This combined with the high-power draw has created situations where the specific heat flux is very high. For example, computer processors typically have a thermal design power (TDP) of 100 W and even upwards of 250 W [1, 2] which is dissipated over an area of less than 20 cm^2, thus resulting in a specific thermal flux of about 10-15 W/ cm^2. In the application of power electronics, the specific thermal flux is in the order of 1000 W/ cm^2 [3]. In the field of renewable energy, the specific thermal flux is, in the applications of concentrator photovoltaics, in the order of 1370 kW/m^2 [4] with potential to reach values greater than 10000 kW/m^2 [4]. The issues due to limitation of heat dissipation that arise in the above cases have directly led to the push towards development of new and novel solutions. One such method that has garnered a lot of attention is the use of microchannels.

Microchannel based heat sinks have been studied in various configurations to improve the heat dissipation characteristics of cooling solutions employed in a wide variety of applications which content with high heat flux dissipation issues. They have been used extensively in the electronics industry; medical, consumer grade micro-electronics, military & space applications, refrigeration & cryogenic applications, solar cells to name a few [5, 6]. Microchannels can be defined as elements which can be used for heat transfer where the classical theories cannot accurately establish the friction factor and heat transfer. Alternatively, it can also be defined a microscale system as one whose typical phenomena are typically not observed in a macro system [7]. There has been some debate regarding the exact definition of what constitutes a microchannel. However, in general, they can be described as fluid flow paths which have a hydraulic diameter less than 1 mm [7, 8]. We can illustrate the effectiveness, advantages, and the rough theory behind the use case of single-phase flow microchannels by applying the classical relationship (1) developed for channels in macroscopic scale. Here h is the convective heat transfer coefficient of the flow, d is the hydraulic diameter, and k is the thermal conductivity of the fluid.

$$Nu = \frac{h \cdot d}{k} = const \Rightarrow h \propto \frac{1}{d} \tag{1}$$

✉ Prasenjit Dey
prasenjit.dey@nitgoa.ac.in

[1] Department of Mechanical Engineering, National Institute of Technology Goa, Ponda Goa – 403401, India

Considering a laminar flow which is fully developed and with a constant Nusselt number, implying that the HTC (heat transfer coefficient) is mathematically inversely proportional to the diameter [8]. This is an indicator of the performance potential of microchannel systems. Microchannels have been shown to offer measurable benefits over other heat transfer systems. Microchannels have been shown to have superior heat transfer performance, far more compact and lightweight, reduced heat sink size, low rate of coolant flow, larger available heat transfer area per unit fluid flow volume and uniform wall temperature distributions [9, 10]. Experimentation on microchannel systems have shown that they offer elevated heat dissipation capabilities with values exceeding 10000 kW/m^2 which can be efficiently dissipated with the help of flow boiling regime via latent heat transport [11].

The sections below, we attempt to summarize some of the different microchannel structures and geometric designs of microchannels popularly used. The advantages, disadvantages, and the suitability of different geometries in microchannels are elucidated. Different phase regimes used along with use of nanofluids in microchannels are also explored and the advantages, disadvantages and challenges faced in each listed. Applications of microchannels are also listed and progress in each domain is reviewed. Lastly, the challenges and future prospects for MCHS are offered. This review aims to be an effective guide for future advancement of high-performance MCHS.

2 Structure and geometric design of microchannels

The structure and geometry of microchannels heavily influence the performance they offer. Extensive research has been done into gaining understanding of that mechanisms of heat transfer in microchannels. Effects of thermal boundary layer, fluid mixing, flow velocity etc. have been studied [5]. In order to reduce pumping losses and large pressure gradients, several geometries of microchannels have been explored concurrently. This paper aims to look at some of the widely used microchannel structures in both the single and multi-phase flows.

2.1 Straight channels

As the name suggests, straight cut microchannels are microchannels whose profiles are manufactured along a straight locus. The profiles themselves may be of different shapes.

Kumar and Kumar [12] carried out 3-D numerical simulations on rectangular MCHS with arc shaped grooves to examine the fluid flow and transfer of heat characteristics.

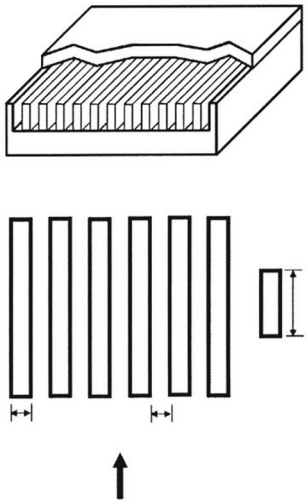

Fig. 1 Structure of MCHS [18]

Groove depth along with the Reynold's number were varied and Nusselt number, Poiseuille number, and performance factor were analysed to compute the effect of groove structure and depth on the hydrodynamic and thermal characteristics of the microchannel. Grooves were found to result in the generation of pseudo secondary flows which had an impact in reducing the viscous forces in laminar region but had no effect with higher Reynold's numbers and actually reduced effective heat transfer. Law and Lee [13] conducted analysis comparing pressure and flow boiling and heat transfer characteristics in straight microchannels. FC-72 dielectric fluid was used, and results indicated a reduced pressure drop in straight finned microchannels as compared to oblique microchannel.

Alam et al. [14] and John Mathew et al. [15] conducted comparative analysis to characterize flow boiling heat transfer and pressure drop in micro gap and MCHS (microchannel heat sinks). While investigating micro gap heat sinks, the study showed that MCHS had superior performance with

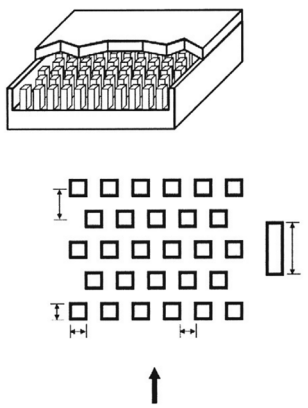

Fig. 2 Structure of MPFHS [18]

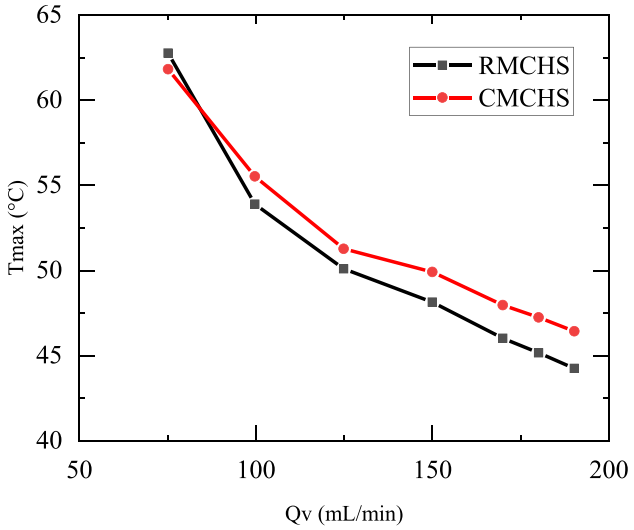

Fig. 3 Maximum temperature of heater surfaces plotted against flow rate for two heat sinks at Power of 48 W. [19]

regards to heat transfer at small heat flux caused due to early formation of slug/annular flow. Balasubramanian et al. [16, 17] investigated heat transfer during flow boiling, pressure drop and instabilities in straight and expanding microchannels. Observations indicated that pressure drop (lower by 30%), wall temperature fluctuations and was lower in expanding microchannels with greater observed heat transfer performance. Thin film evaporation was determined to be the predominant mechanism of heat transfer with high heat fluxes. In straight microchannels, lower heat transfer coefficients were observed when the pressure drop fluctuations amplitudes rose.

Jasperson et al. [18] conducted research comparing microchannel (MCHS) (Fig. 1) and micro-pin-fin heat sinks (MPFHS) (Fig. 2) focusing on the thermo-hydraulic performance & also considering the manufacturability. It was determined that MPFHS have superior performance (lower thermal resistance) at flow rates above 60g/min albeit with a greater pressure drop penalty (nearly double) as compared to MCHS. In terms of manufacturability, casting (for mass production) would yield a similar costing. However, for prototyping in which micro-end milling and micro-EDM are utilized, microchannels are the more cost-effective option as the tool path (thus machining time & tool life) is nearly a third that require for micro-pin-fin manufacturing.

Xia et al. [19] researched the characteristics of flow and heat transfer in rectangular and staggered complex corrugated microchannels experimentally as well as numerically. Pressure drop was found to be greater for rectangular microchannel heat sinks (RMCHS) as compared to the staggered complex corrugated channel microchannel heat sinks (CMCHS). However, heat transfer characteristics were superior in CMCHS as compared to RMCHS with the maximum and average temperatures being lower for higher flow rates. Figure 3 shows variation of average temperature on heater surface with rate of flow for two heat sinks at 48W. Observations indicate that the average temperature reduces with a rise of rate of flow for both the heat sinks. The maximum temperature of CMCHS was below that observed in RMCHS when flow rate was greater than 80 ml/min. However, the reverse was true when flow rate was less than 80 ml/min. The average temperature observed in CMCHS in comparison with RMCHS is lower by approximately 1.2 °C.

S.N.	Reference	Enhancement	Solution Method	Dimensions	Working Fluid	Operating parameters	Enhancement Effect
1	Kumar and Kumar [12]	Straight MC	Num.	W = 231 µm H = 5637 µm D_h = 348.9 µm	Water	Re = 200, 900, and 2000 T_{in} = 300 K Pr = 6.99	Groove present on the floor and both the side walls raised the Nusselt number by 119% as compared to the plain walled MCHS At higher Re, the increase in groove depth decreases the effective heat transfer
2	Law and Lee [13]	Straight and Oblique	Expt.	W = 0.30mm H = 1.2mm 25 x 25 mm, 40 MC, 0.30 mm fin thickness	FC-72	5 Readings: Q_v = 175 - 350 kg/m^{2}s T_{in} = 29.5 °C	Straight: 1.7x Lower pressure drop caused by the sudden change in the flow direction, where fluid is being forced to flow through secondary channels Oblique: HTC: 1.2-6.2 times greater CHF: 2.5-2.8 times greater Pressure instabilities: 4x lower Caused by disruption of the liquid thin film by the secondary oblique channels

S.N.	Reference	Enhancement	Solution Method	Dimensions	Working Fluid	Operating parameters	Enhancement Effect
3	Alam et al. [14]	Microgap and MCHS	Expt.	W = 12.7mm $H_{microgap}$ = 190.34μm H_{MC} = 385.70 μm test piece= 12.7 x 12.7 mm	DI water	q = 0 - 85 W/cm^2 (increments of 10) G = 400 - 1000 kg/m^2 s T_{in} = 86 °C	Higher HTC, Lower Pr. Drop, pr. Fluctuations, wall temp and fluctuations, hotspot temp For Microchannel vs Microgap
4	Mathew et al. [15]	Hybrid MC-Microgap Heat Sink, Conventional Straight MCHS and Microgap Heat Sinks	Expt.	W = 338μm H = 568μm Test piece: 25 x 25mm	DI water	T_{in} = 85.5 °C, 0-128 W/cm^2 (steps of 1.6 W/cm^2 close to ONB, 4 W/cm^2 at higher heat flux conditions) G = 100, 150, 199, 299 kg/m^{2}s	Hybrid improves boiling stability, HTC remain stable or gradually increase even at the highest heat flux,
5	Balasubramanian et al. [16]	Straight and expanding MCHS	Expt.	$W_{Straight}$ = 322.5 μm $W_{Expanding}$ = 304.5 - 2115.2 μm $H_{Straight}$ = 1153.1 μm $H_{Expanding}$ = 1190.1 μm Test piece = 25 x 25 mm	DI water	G = 100 - 133 kg/m^{2}s $T_{inlet, water}$ = 90 °C q < 140 W/cm^2	Pressure drop lower 30% in expanding MC, more stable, lower wall temp
6	Miner et al. [20]	Expanding microchannel array	Expt.	W = 156.8 -162.8μm H = 591.4 -1046.1 μm	Refrigerant R-134a	Q = 527 W G = 2 - 4 g/s	CHF_{max} appears for both 2 g/s and 3 g/s nominal flow rates CHF_{max} moves right, toward greater expansion, as the flow rate increases
7	Lee et al. [21]	MCHS with divergent channels	Expt.	W = 235 μm H = 710 μm D_h = 353 μm	Water	q = 6 – 38 W/cm^2 inlet subcooling 5 – 30 °C x_{exit} < 0.24 G = 25, 41.8, 65.2, 114 kg/m^{2}s	expanding micro-channels and the installation of inlet orifices could prevent the channel instability
8	Jasperson et al. [18]	Comparison of Micro-Pin-Fin and MCHS	Num.	W = 200 μm H = 670 μm	Water	Q_v = 35-85 g/min Tin = 30 °C and 60 °C	For Q_v < 60 g/min, MPFHS has a higher thermal resistance than MCHS, pressure drop approximately twice as large at low rates
9	Xia et al. [19]	MCHS with complex structure	Comb. Expt. & Num.	W = 300 μm For single corrugated channel: $W_{minimum}$/ $W_{maximum}$ = 0.1/0.2 mm pitch = 0.2 mm H = 0.975 mm	DI water	Q_v = 75-190 ml/min Q = 42-66W	Pressure drop of CMCHS is larger than RMCHS Heat transfer is enhanced for CMCHS Total thermal resistance of CMCHS is reduced by 18.99%
10	Xie et al. [22]	MCHS with internal vertical Y-shaped bifurcations	Num.	W = 315 μm H = 400 μm	Water	V_{in} 0.66, 0.8, 1.00, 1.32 and 1.6 m/s T_{in} 297 K, q = 24.49 W/cm^2	25 mm internal Y-shaped bifurcation microchannel shows the best thermal performance with thermal resistance decreased 41.02%

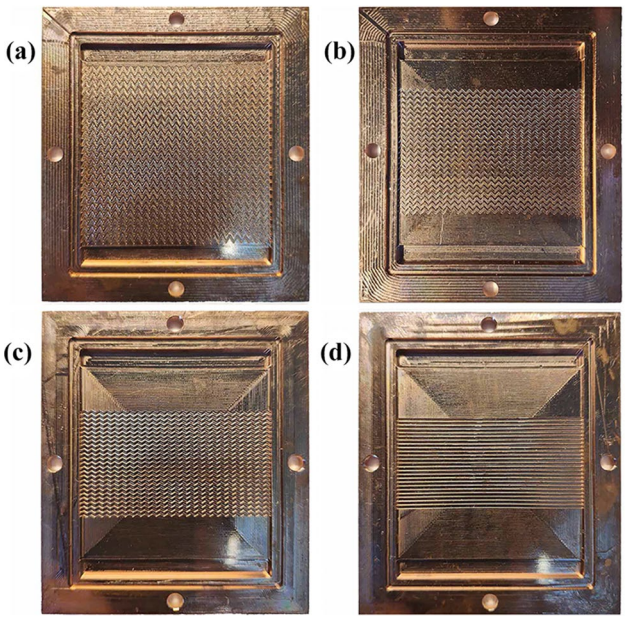

Fig. 4 Zigzag microchannel of ZSMHS: (**a**) α = 30°, (**b**) α = 45°, (**c**) α = 60°, (**c**) α = 90° [25]

2.2 Wavy channels

It has been determined that utilization of wavy walls (or corrugations) in heat exchangers can improve characteristics of heat transfer. This is attributed to superior mixing of the fluid by the wavy surfaces. This is even more important in the current scenario where even greater levels of improvement in heat exchanger performance is pursued to meet the ever-increasing industry requirements and calls for greater heat transfer performance.

While Mondal et al. [23] studied the fabrication of wave microchannels, Aliabadi et al. [24] researched the flow and heat transfer characteristics observed in chevron channel MCHS using numerical simulations. The results were promising and showed a noticeable increase in thermal performance and reduced thermal resistance. Peng et al. [25] examined the performance of zigzag serpentine microchannel heat sinks (ZSMHS) (Fig. 4) by experimentally determining the heat transfer characteristics. They found that lower incidence angles, lowered the drop in pressure and friction coefficient with the lowest values being observed at 30° and the maximum at 90°. Also, the reduction in incidence angles improved the heat transfer performance (heat transfer coefficient & thermal resistance).

G.D. Xia et al. [26] researched the effects of different geometric structures in MCHS on the heat transfer and fluid flow characteristics with numerical techniques. Optimal geometric parameters for greatest heat transfer and flow distribution were determined by studying the effects of different types of inlet and outlet configurations, header shapes and along with different microchannel shaped (Fig. 5). It was determined that average temperature and maximum temperature of the heat sink A was higher as compared to the values determined for heat sink B and C.

Zhou et al. [27] performed optimization of geometric parameters of a wavy wall (Fig. 6) by combining response surface methodology (RSM) with finite volume method (FVM) simulation. β (Comprehensive heat transfer index) was used to investigate if the augmentation of heat transfer offsets the rise in the drop in pressure. The impacts of amplitude and wavelength of wave, Reynolds number and β were investigated. It was observed that as the Re numbers increases proportionally with the convective HTC. It was observed that heat transfer was up to 2.8 times greater in wavy microchannels as compared to straight microchannels. An increase of Re number results in increase of pressure drop for all geometries with a greater drop in pressure in wavy MCHS. Using the aforementioned methods, it was determined that the optimal amplitude was 40 μm and wavelength 100 μm.

S.N.	Reference	Enhancement	Solution Method	Dimensions	Working Fluid	Operating parameters	Enhancement Effect
1	Aliabadi et al. [24]	Chevron MCHS	Comb. Expt. & Num.	4 designs investigated: Width = 1 mm Height = 1 mm	Water	Re=50-300 q= 100 kW/m^2	Novel patterns impact the flow behaviour of the fluid and enhance the thermal performance Thermal resistance decreases as the number of curvatures increases
2	Peng et al. [25]	Zigzag serpentine MCHS	Expt.	W_{Zigzag}= 0.8 mm $W_{serpentine}$ = 0.5 mm H_{Zigzag} = 0.1 mm $H_{serpentine}$ = 0.8 mm Incidence angles = 30°, 45°, 60°, 90°	DI water	T_{in}=20 °C For Q_v = Const.: heat source is 50 °C, 55 °C, 60 °C, 65 °C, 70 °C and 75 °C, For const. heat source: G=10-45 g/min (Re<2320) 14.1 W ≤ Q ≤ 80W	Low pressure drop and friction coefficient lowest at 30° and the max at 90°

S.N.	Reference	Enhancement	Solution Method	Dimensions	Working Fluid	Operating parameters	Enhancement Effect
3	Xia et al. [26]	Wavy v/s Straight with different header designs	Num.	A (L1/W3 = 40) B (W4/W3 = 0.5, R/W3 = 1, L5/W3 = 2.5) C (L4/W3 = 2, W5/W3 = 2)	Water	q_w = 200W/cm^2	MCHS with offset fan-shaped reentrant cavities and with triangular reentrant cavities augment the heat transfer compared to conventional rectangular MCHS
4	Zhou et al. [27]	MCHS with wavy channel	Num.	W_c = 85 µm H_r = 100 µm A =10 - 40 µm λ = 100, 550, 1000 µm	Water	V_{in} = 0.6, 0.8, 1, 1.2, 1.4 m/s q = 100 W/cm^2 T_{inlet} = 298 K	Optimization studies done
5	Ahmed et al. [28]	Wavy channel	Num.	A = 0, 0.1, 0.2 and 0.3 λ = 2.2, 2.8 and 3.6.	copper–water nano-fluid	Re = 100 – 800 Φ = 0 – 5%	enhancement in HTC depends mainly on Φ, A and Re rather than the λ

2.3 Pin fins

Structures used in Micro pin fin heat sinks (MPFHS) have demonstrated the ability to disrupt and also re-develop boundary layers, while also increasing flow mixing via vortices [9]. Feng et al. [29] conducted a numerical investigation of the geometrical parametric effects of circular MPFHS to effects on heat transfer and fluid flow in an interrupted MCHS. The author worked on an interrupted microchannel with double circular pin-fins in each microchamber (IMCDCP). The design aimed to fuse the advantages of microchamber and circular pin-fin in the enhancement of heat transfer. Parameters such as diameters, spacing and height were altered and changes in the Nusselt's and Reynold's numbers were recorded. IMCDCP was found to improve heat transfer and reducing wall temperature. As compared to smooth microchannels, the IMCDCP with height of 0.08mm, pin-fin diameters of 0.12 mm, channel width of 0.55 mm operating under conditions yielding Reynold's number of 530, resulted in a 42% heat transfer performance improvement over smooth microchannels setup.

Ferster et al. [30] investigated the effects of spacing, geometry and fin count of pin-fins in additively manufactured MPFHS. The arrays of triangular, star, and spherical pin-fins (Fig. 7) were fabricated using direct metal laser sintering (DMLS) technique. Results indicated that triangular and cylindrical geometries had the greatest values for augmentation of heat transfer. Streamwise spacing had a small but measurable effect on friction factor and a direct correlation with performance with regards to heat transfer (with decreasing spacing).

Jasperson et al. [18] performed comparative studies between MCHS and MPFHS (Fig. 8) taking into account thermo-hydraulic performance as well as its' manufacturability. Above 60 g/min, the thermal resistance of HPFHS was

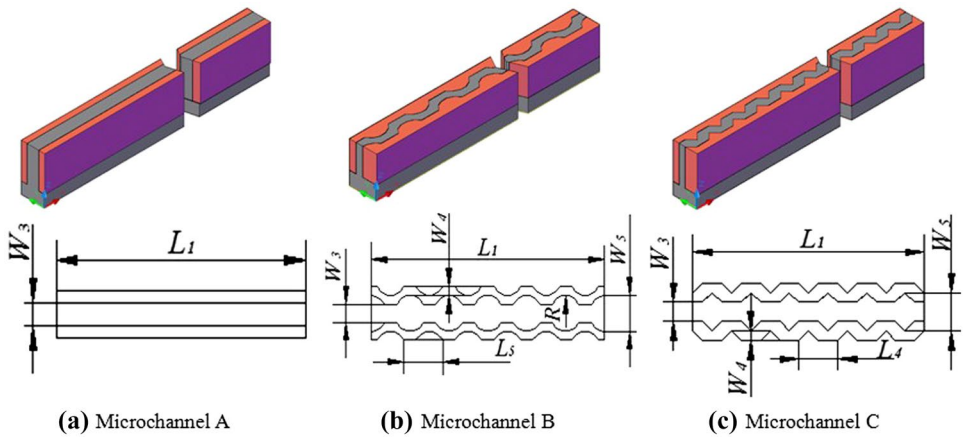

(a) Microchannel A (b) Microchannel B (c) Microchannel C

Fig. 5 Different microchannels investigated [26]

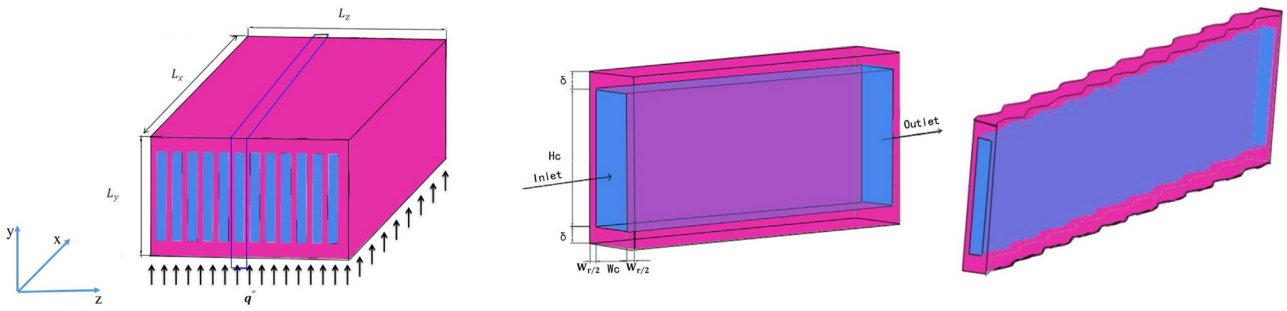

(a) (b) (c)

Fig. 6 Schematics of (**a**) MCHS, (**b**) straight MCHS and (**c**) wavy MCHS [27]

observed to fall below that of MCHS. The more complicated flow and strong vortices in the wake at high flow rate was attributed. Thus, the HPFHS can be chosen in such operating conditions. While methods for prototyping like micro-EDM, micro-end-milling etc. result in higher manufacturing costs, methods used in mass manufacturing such as casting and extrusion result in cost parity. Moreover, ongoing research in spindle speeds and feed rates suggests that cost for prototyping itself would reduce, thus resulting in comparable costing during prototyping phase as well.

Lan et al. [31] determined the hydrothermal performance & entropy generation of rectangular microchannels with offset and truncated pin-fins with variable fluid properties. As observed in earlier cases, as compared to smooth MCHS, MPFHS enhance the performance with regards to heat transfer. This was attributed to extension of area available for transfer of heat, redevelopment of thermal boundary layer and generation of vortices. However, there is an increase in resistance to fluid flow. There is a correlation between the increase in pin-fin length and the increase in resistance to heat transfer and increased flow. While offset in pin-fins can increase heat transfer up till a point, beyond which there is a reduction (Fig. 9). In Fig. 9 for MC–0.75–0, no offset value exists for adjacent pin-fins, thus the equal area was available for fluid flow on either side of each pin-fin. With offset, two adjacent between pin-fins ($W_{rc} > 0$), on either side of each pin-fin, different sizes of flow passage were formed. Thus, greater volume of fluid passed through the side with the larger flow passage. Values of PEC were found to vary from 1.00 to 1.43. The highest value of PEC achieved was 1.43 for microchannel MC–0.75–0.6 ($W_{rc} = 0.6$) at Re = 530.

Soleymani et al. [32] worked on a hybrid design viz microchannels with pin fins (rounded rectangular & NACA 0024 air foil) at hotspot region (Fig. 10). Different pitch angles were also looked at for the air foil shape relative to fluid flow direction (Fig. 11). It was seen that rectangular pin fin and higher angles of air foil pin-fin had lower thermal resistance albeit with greater pumping power requirements. Tillius et al. [33] conducted optimization studies of short micro pin-fins in MCHS.

S.N.	Reference	Enhancement	Solution Method	Dimensions	Working Fluid	Operating parameters	Enhancement Effect
1	Alam et al. [34]	Triangular Pin fins	Num.	W = 12.5D H = 0.4h d = D/e = 0.4 and 0.8	Air	T_{in} = 300 K q = 2.0 kW/m^2 Re = 500 - 10000	The highest Nu value at d = 0.8 are 97.43, 91.25, 83.81 and 74.47 for TI = 20%, 15%, 10% and 5%
2	Bhandari et al. [35]	Square Pin fins	Num.	W_c = 1 mm H_f = 0.5 – 2.0 mm W_{Fin}= 1 mm (Square)	Water	q = 75-150 kW/m^2 Re = 100 - 800	Optima at 1.5mm
3	Feng et al. [29]	circular pin-fins	Num.	W = 0.1 mm H = 0.2 mm d_1 (pin-fin in upstream) = 0.06 – 0.14 mm d_2 (pin-fin in downstream) = 0.06 – 0.14 mm s (between double circular pin-fins) = 0.25 –0.85 mm $h_{circular\ pin\text{-}fin}$ = 0.04 – 0.2 mm	Water	u_{in} = 1–4 m/s T_{in} = 293 K q = 10 MW/m^2	Lower local wall temperature and better wall temperature uniformity, heat transfer enhancement in comparison with SMC Greater pin-fin diameter in microchamber lowers the local wall temperature, improves heat transfer enhancement, increases pressure drop and larger friction losses

S.N.	Reference	Enhancement	Solution Method	Dimensions	Working Fluid	Operating parameters	Enhancement Effect
4	Ferster et al. [30]	Triangle Star, Dimpled sphere, Cylinder pin fins	Expt.	H =1.0 mm $D_{Triangle}$ = 0.93 mm, D_{Star} = 2.2 mm, $D_{Dimpled\ sphere}$ = 1.44 mm, $D_{Cylinder}$ = 1.0mm S/D = 1.5, X/D = 1.3 S/D = 1.5, X/D = 2.6 S/D = 2.0, X/D = 2.6 S/D = 4.0, X/D = 2.6	Air	Re = 300 - 30,000	Triangular and cylindrical geometries had highest heat transfer augmentation Streamwise spacing directly affected heat transfer
5	Jia et al. [36]	cone-shaped micro pin fins	Num.	W_c = 0.2 mm H_{ch} = 0.2 mm L1 = 0.2 – 0.8 mm	DI water	$T_{in} = T_f$ = 293 K P_{out}= 0 q= 10 MW/m^2 Re = 150-650	Overall thermal performance of MCPF is better than Rec microchannel
6	Lan et al. [31]	truncated and offset pin-fins	Num.	W = 0.1 mm H = 0.2 mm $L_{pin\text{-}fin}$ = 0.06 mm $W_{pin\text{-}fin}$ = 0.03 mm H_r = 0 – 0.2 mm offset value (W_r) = 0 - 0.07mm		u_{in} = 1–4 m/s Re = 132 - 530 T_{in} = 293 K q = 10 MW/m^2	H_{rc} = 0.75 and W_{rc} = 0.6 had thermal performance, maximum overall thermal performance factor= 1.43 at Re= 530
7	Mei et al. [37]	micro-pin-fin arrays at low Re in micro-reactors	Comb. Expt. & Num.	W_c= 18 mm hf = 1, 1.1, 1.2, 1.5, 2 mm W_{pin} = 1 mm Pitch = 1.8 mm	DI water	Q_v = 1 to 25 L/h T_{in} = 298.15 K P_{in} = 0 Pa U_{in} = 0.008 - 0.2 m/s	Tip clearance of h_c/h_f = 1.1 or 1.2 had highest heat transfer performance as compared to those without
8	Saravanan and Umesh [38]	Comparison of Micro-Pin-Fin and Microchannel Heat Sinks	Num.	**MCHS Unfinned**: W_c = 0.75 mm, Hch = 1 mm, **MCHS finned**: W_c = 0.75 mm Hch = 1 mm **Square pin fin** 0.5 x 0.5 mm, height = 0.5 mm **Circular pin fin** diameter = 0.5 mm, height 0.5 mm, spacing S_x = 0.125 mm and S_z = 0.5 mm	Water	T_{in} = 293 K Re = 100-900 q = 10 W/cm^2	Highest thermal resistance observed in MCHS/SPF, lower by 42% compared to HS/SPF and for MCHS/CPF lower by 57% compared to HS/CPF

2.4 Oblique

Oblique microchannels are those which have straight microchannels parallel to the direction of the flow and have (secondary) oblique cuts at an angle to the original (Fig. 12). Oblique fins have several advantages. They can augment heat transfer by modulating the flow, and by breaking the boundary layer and causing it to be reinitialized periodically thus reducing the thermal boundary layer thickness. Also, the secondary flows created by the obliquely positioned channels improve mixing of the fluid increasing the HTC by as much as 80% (Fig. 13) [39–42].

Lee et al. [39] researched the enhancement of thermal dissipation in MCHS with the utilization of oblique fins. Using numerical simulations, it was determined that by adjusting the sizing of the secondary channels, an adequate supply of flow (in this case, 12%) could be diverted so as to disrupt the boundary layer whilst causing a negligible pressure to drop. Ansari et al. [43] performed comparative and optimization studies using numerical techniques on oblique and rectangular fin MCHS both with parallel and offset fins. It was found that oblique-fin offset MCHS have the lowest thermal resistance at the equivalent pumping power. Law and Lee [44] conducted comparative (experimental) studies between straight

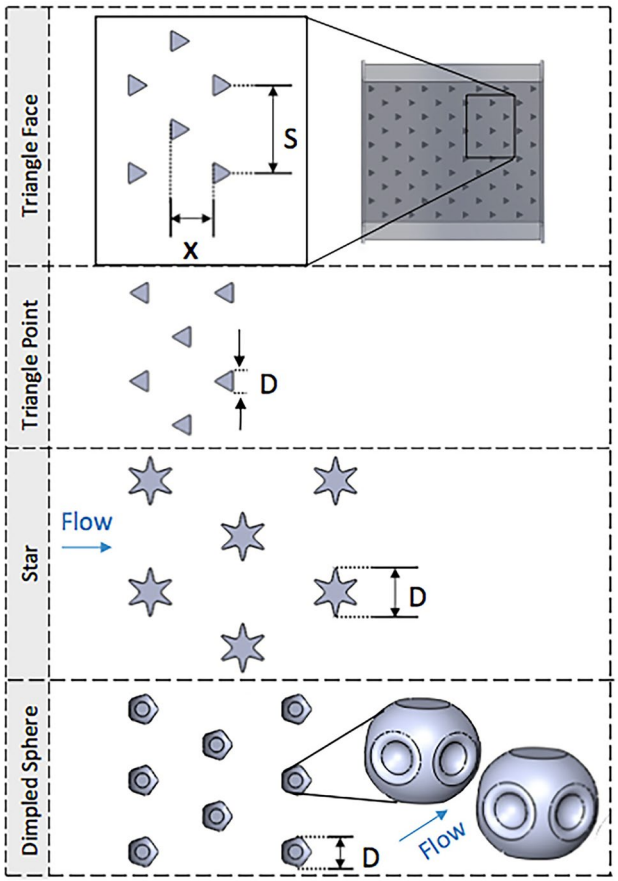

Fig. 7 2-Dimensional models for each pin shape [30]

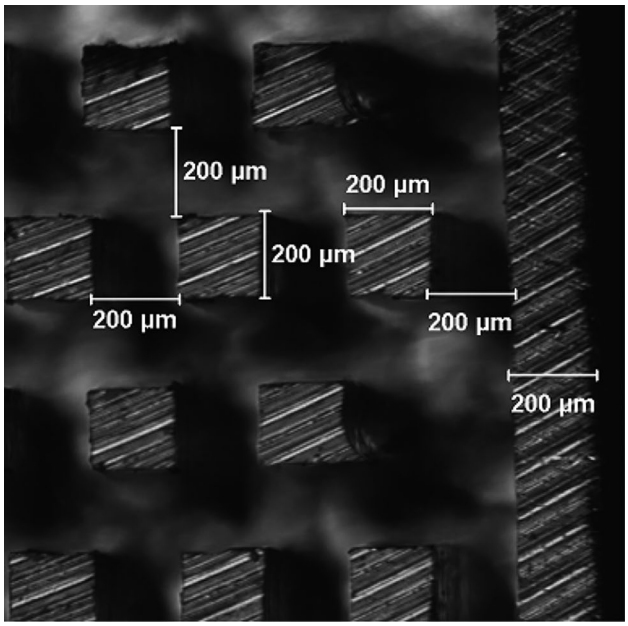

Fig. 8 MPFHS manufactured by micro-end-milling [18]

and oblique finned (10°) microchannels to analyse temperature and pressure instabilities. It was determined that the temperature and pressure instabilities present in RSMCs are generally mitigated in obliquely finned microchannels while also augmenting heat transfer characteristics. The improved flow stability observed is linked to the ability of oblique fins to reduce flow reversals. Law et al. [45] conducted studies looking at the impact of altering the oblique angles (10°, 30°, 50°) on the pressure and flow boiling characteristics in oblique finned MCHS. Heat transfer was observed to rise with increase in oblique angle due to reduction of flow rates in the secondary channels. A considerable rise in pressure drop with rise in angle from 10° to 30° and marginal rise from 30° to 50° was seen. Lee et al. [46] investigated the use of obliquely finned microchannels for hotspot mitigation. A group of oblique fins with a dissimilar pitch and higher density were created at regions where hotspots were expected (Fig. 14). This resulted in additional secondary flow and thus greater boundary layer redevelopment which provided more effective heat dissipation capability at region with high flux.

Lee et al. [47] performed a parametric study to enhance fluid flow and heat dissipation in obliquely finned MCHS. It was determined that the optimum performance was obtained using a channel width of 100 µm and an oblique angle of 27°. Mou et al. [48] researched the effects of flow migration in obliquely finned microchannel arrays on flow and heat transfer. As from other authors, heat transfer performance was determined to be affected by variations of secondary flow. Reynold's number was found to affect coolant migration, flow stability and heat transfer performance. With higher values of Re enhancing heat transfer for surfaces in secondary channels. Vinoth et al. [49–51] investigated the effects of various channel cross section (square, semicircular and trapezoidal), as shown in Fig. 15, on the heat dissipation and flow characteristics of obliquely finned MCHS. Trapezoidal cross section microchannels (as compared to square and semicircle respectively) were found to have the highest Nusselt number increased by 8.54% and 26.4% and rate of heat dissipation by increased 3.13% and 5.87% albeit with an increased pressure drop (due to higher friction factor) of by 24% and 16.8%. Addition of nanoparticles increased the heat transfer rate by 4.6%.

Lan et al. [52] performed an experimental and numerical examination on the temperature uniformity of different oblique MCHS. The types investigated were variable density alternating obliquely truncated microchannel (AOT-MC), traditional rectangular straight microchannel (RS-MC), and varying density alternating obliquely truncated microchannel with oblique fins (AOTF-MC) as shown in Fig. 16. The enhanced design AOTF-MC showed an increase of up to 63.23% and 111.59% for the Nusselt number and 40.20% and 55.16% reduction for the temperature in comparison with the AOT-MC and the RS-MC, respectively.

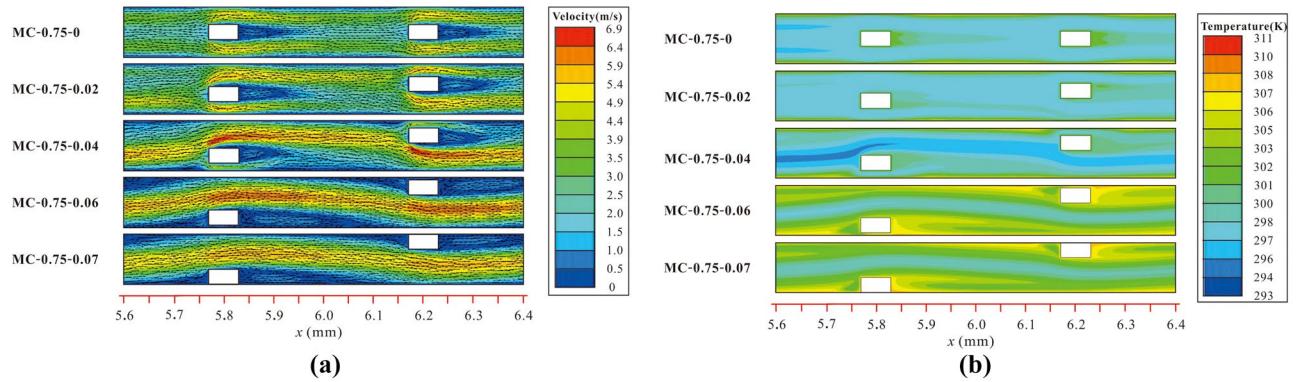

Fig. 9 (**a**) Velocity profile and (**b**) temperature profile for microchannels at various W_{rc} at Re = 397 and H_{rc} = 0.75 (y = 0.2 mm) on x–z plane [31]

Panse et al. [53] conducted a study on an alternating offset oblique microchannel (Fig. 17) to determine its thermos-hydraulic performance using a numerical parametric study. Over a range of Reynold's numbers (200-800), 3 parameters; relative oblique channel width (α), and oblique angle (θ), relative fin offset width (β), on thermo-hydraulic performance (THP) were evaluated. The optimal geometry was found, α=0.5, θ=60°, and β=0.25, obtained the maximum THP of 2.41 at Re=800. Far et al. [54] studied the impact of variation of pin-tip clearance on the oblique finned microchannel performance (numerically) with a nano encapsulated phase change material (NEPCM) slurry at different concentrations. Results indicated that NEPCM slurry enhanced the cooling performance but increased the Euler number. Tip clearance ratio of 0.2 - 0.375 with NEPCM slurry and 0.16-0.26 with water were found to be optimal.

S.N.	Reference	Enhancement	Solution Method	Dimensions	Working Fluid	Operating parameters	Enhancement Effect
1	Lee et al. [39]	Comparison of Oblique and MCHS	Num.	$W_{oblique\ fins}$ = 100 µm $W_{Conventional}$ = 100 µm H_c = 400 µm Fin pitch, p = 300 µm Oblique angle, θ = 26.6°	Water	U_{in} = 1 m/s q = 100 W/cm^2	Combination of the entrance and secondary flow effect improved heat transfer performance (the average and local heat transfer coefficients enhanced by upto as 80%)
2	Ansari et al. [43]	Comparison and optimization oblique-and rectangular-fin MCHS	Num.	W_{ch} = 0.01 m h = 0.0005 m		T_{in} = 300 K q = 10 MW/m^2 G = 0.002 - 0.008 kg/s	Oblique-fin offset MCHS have the lowest thermal resistance at the equivalent pumping power
3	Law & Lee [44]	Comparison of Straight- and 10°Oblique-Finned MCHS	Expt.	$W_{ch,\ Straight}$ = 0.346 mm $W_{ch,\ Oblique}$ = 0.318 mm H_{ch} = 1.185 mm $t_{fin,\ straight}$ = 0.262 mm $t_{fin,\ oblique}$ = 0.292 mm	FC-72	Q_v = 100, 200 ml/min T_{in} = 29.5 °C q_{in}= 14 -42 W/cm^2	Temperature and pressure instabilities in straight-finned microchannels are more severe
4	Law et al. [45]	Varying oblique angles	Comb. Expt. & Num.	W_{ch} = 0.30, 0.32, 0.30, 0.30 mm (nominal, 10°, 30°, 50°) H_{ch} = 1.20, 1.18, 1.19, 1.19 mm (nominal, 10°, 30°, 50°) Oblique-cut width, w_{ob} = 0.15 mm	FC-72	G = 194, 290, 386 kg/m^{2}s T_{in} = 29.5 °C q_{in} = 14 - 70 W/cm^2	Heat transfer increased with increase in oblique angle caused by reduction of flow rates in the secondary channels Pressure drop with increase in angle from 10° to 30° and marginal rise from 30° to 50°

S.N.	Reference	Enhancement	Solution Method	Dimensions	Working Fluid	Operating parameters	Enhancement Effect
5	Mou et al. [48]	Oblique fin microchannel array	Num.	W_{ch} = 0.113 mm H = 379 µm p = 0.405 mm l = 0.292 mm w_{ob} = 0.049 mm θ = 26.3° W_w=0.087	Water	Re = 250 - 660 q_{in} = 25 - 274 W/cm^2	Heat transfer performance was determined to be affected by variations of secondary flow
6	Vinoth and Kumar [49]	Oblique finned MCHS	Expt.	W_c = 900 µm (All) H = 800µm (All) $W_{fin\ Semi\text{-}circular}$ = 800 µm $W_{fin,\ Square}$ = 800 µm $W_{fin,\ Trapezoidal}$ = 900 µm L = 1000 µm Fin pitch, P = 800 µm Oblique angle, θ = 26°	H_2O and Al_2O_3/H_2O nano-fluid of volume fraction 0.25%	Q = 80 W G = 90 - 480 kg/m^{2}s	Trapezoidal cross-section results in higher Nusselt number by 8.54% and 26.4%and heat transfer rate by 3.13% and 5.87% than square and semicircle Trapezoidal CS has greater pressure drop by 24% and 16.8% more than semicircle and square CS Nanofluid exhibits greater the heat transfer rate by 4.6% when compared with the water
7	Vinoth and Kumar [49]	Oblique finned MCHS	Expt.	W_c = 900 µm (All) H = 800µm (All) $W_{fin\ Semi\text{-}circular}$ = 800 µm $W_{fin,\ Square}$ = 800 µm $W_{fin,\ Trapezoidal}$ = 900 µm L = 1000 µm Fin pitch, P = 800 µm Oblique angle, θ = 26°	H_2O and Al_2O_3/H_2O nano-fluid of volume fraction 0.25%	q = 5.5 - 26.5 kW/m^2 Q_v = 0.1 LPM	Trapezoidal cross-section performs better, and provides 8.5 and 10.3% increased heat transfer rate than square and semi-circle cross sections respectively
8	Lan et al. [52]	Variable density alternating obliquely truncated microchannel	Comb. Expt. & Num.	W_c = 800 µm (RS) Secondary passage width = 400 µm (AOT, AOTF) H_c = 1200 µm (RS) Obliquely truncated angle θ = 30° (AOT, AOTF)	DI water	Q = 125 W	The enhanced design AOTF-MC showed an increase of up to 63.23% and 111.59% for the Nusselt number and 40.20% and 55.16% reduction for the temperature in comparison with the AOT-MC and the RS-MC, respectively.
9	Panse et al. [53]	Alternating offset oblique microchannel	Num.	W_c = 0.75 mm H_c = 1 mm W_{fin} = 0.75 mm l_{fin} = 2 mm	Water	α = W_0/W_c = 0.33, 0.5, 0.66 β = W_{off}/W_c = 0.125, 0.167, 0.25 θ = 45°, 60° Re = 200-800	Fin offset results in tremendous augmentation in THP which is much more superior to the case of alternating oblique microchannels without fin offset (AOMC) and SMCs Optima at: α = 0.5, β = 0.25, θ = 60°, THP of 2.41 at Re = 800
10	Far et al. [54]	Enhanced MCHS with oblique fins and PCM slurry	Num.	W_c = 0.539 mm H_c = Variable W_{fin} = 0.465 mm l_{fin} = 1.5mm p_{fin} = 2 mm	Nano-encapsulated PCM, DI water	T_{in} = 296:15 V_{in} = 0.250 m/s	Tip clearance ratio of 0.2-0.375 with NEPCM slurry and 0.16-0.26 with water were found to be optimal

2.5 Porous

Porous structures can be introduced in MCHS via surface structures or with the construction of the MCHS itself in a porous manner. Introduction of porous structures has shown to greatly improve the performance of the microchannels [55]. The porous structure provides sites for nucleation and subsequent growth while also increasing area available for heat transfer. This reduces the level of wall superheat for boiling initiation [9]. Sarafan et al. [56] numerically examined mass transfer and thermal dissipation during fluid flow (non-Newtonian power law) in a porous MCHS. It

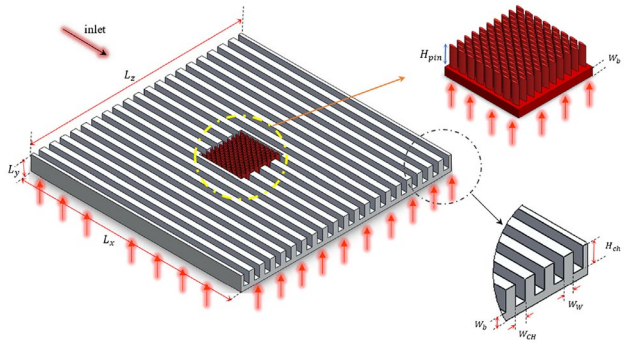

Fig. 10 Microchannel pin-fin hybrid heat sink configuration [32]

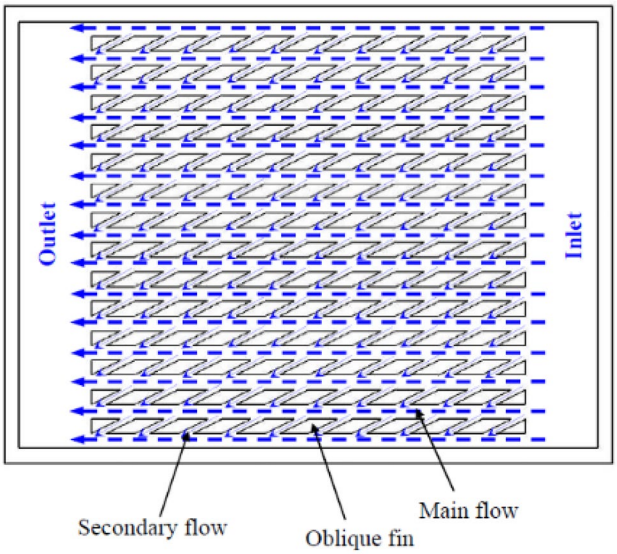

Fig. 12 Plan view of MCHS with oblique fins [39]

was determined that with rising power index, as the fluid tends to thicken and the viscosity increases and thus the shear stress increases, there is a reduction of heat transfer rate. Li et al. [57] determined that convective heat transfer was greatly improved with porous microchannels. This was attributed to the disruption and redevelopment of the thermal boundary layers which was in turn caused by the intensified fluid mixing in porous regions. Dehghan et al. [58, 59] sought to analytically determine the heat transfer performance (HTP) for porous media filled MCHS. To widen the scope of application, several factors were considered (effects of the porous medium shape parameter, the conduction heat transfer within the walls, the slip flow regime, the heat transfer amongst the solid and fluid phases of the porous material, and internal heat generations within the two phases of the porous material). It was determined that using hyper-porous materials greatly enhance HTP. Negligible effects of wall conduction resistance, especially in slip flow regime, on HTP have been deduced. Haddad et al. [60], using numerical techniques, investigated the development of free-convection gas flow in a vertically oriented filled porous medium open-MCHS. It was determined that skin friction, by using modified extended Darcy-Brinkman-Forchheimer model, increased by decreasing Knudsen number and Grashof number, increasing the Darcy number. Also, it was seen that HTC was found to decrease with increase in Knudsen number, in thermal conductivity ratio, reduction in Darcy number, Grashof Number and Biot number. Jia et al. [61] conducted experimental studies to compare flow boiling and pressure drop characteristics in porous wall (PW) and rectangular (Rec) MCHS. PW-MCHS, like in other studies, have a lower temperature superheat. CHF of PW MCHS increase with mass flux and delay premature dryout in comparison to Rec-MCHS. The CHF rise can be attributed to wicking effects created by pin-fin arrangement. Mondal and De [62] attempted to quantify mass transfer in the porous microchannel. Permeation was found to cause rise in mass transfer coefficient by a factor of 5 as compared to impervious walled conduits.

Various configurations of porous materials have also been studied. Zargartalebi et al. [63] examined the flow dynamics and thermal dissipation characteristics in partially porous pin finned (in in-line and staggered configurations) MCHS. It was determined that as the height of the porous media reduced, the flow through the medium was by-passed, more so in the staggered pin-fin configuration than the inline. With higher height of porous media, the reverse is true, that is staggered configuration outperforms the inline configuration.

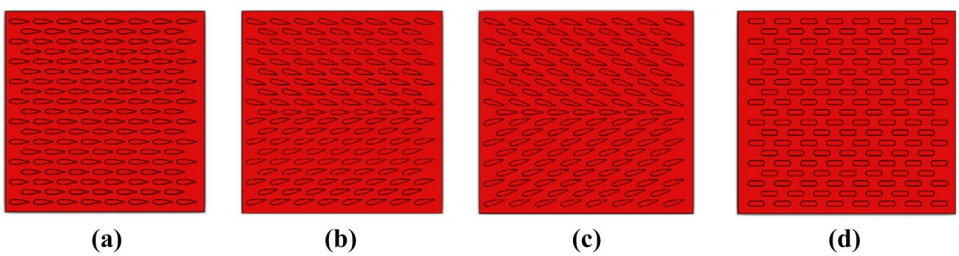

Fig. 11 Various angles used in NACA 0024 airfoil pin-fin (**a**) 0° (**b**) 10° (**c**) 15° (**d**) rounded rectangule pin-fin at zero angle [32]

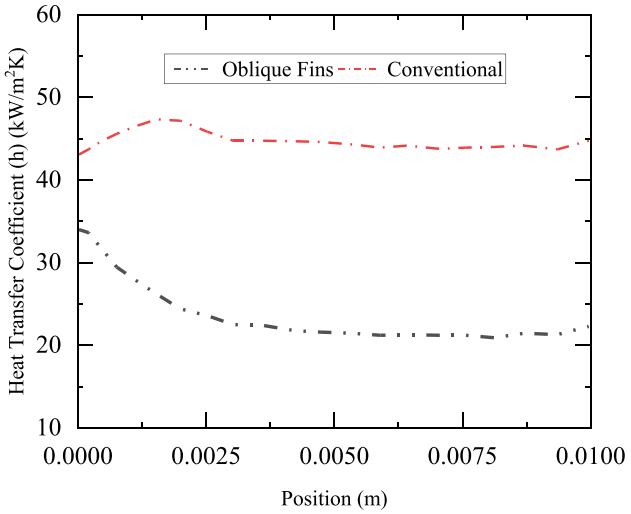

Fig. 13 Local HTC profile for microchannel heat sinks [39]

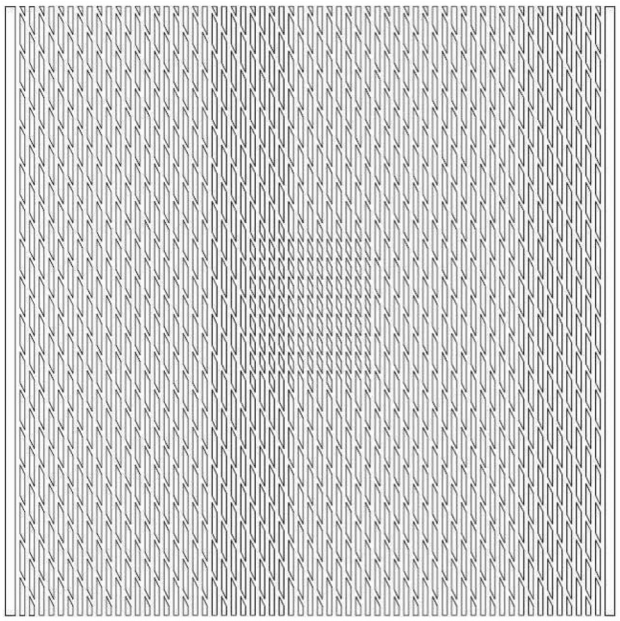

Fig. 14 Design of Heat sink for enhanced variable fin pitch equipped MCHS for single hotspot [46]

The friction ratio of staggered over in-line configuration, at a critical porous height, was found to suddenly increase indicating the forced flow through the medium.

Deng et al. [64] looked to characterize flow boiling observed in porous MCHS with re-entrant microchannels. Use of traditional metal sintering fabrication techniques to manufacture Ω-shaped re-entrant microchannels was done (Fig. 18). Comparisons with solid microchannels showed a significant wall superheat indicating lower thermal impedance, lower boiling instabilities and a 100% - 400% increase in HTC. At low heat fluxes, nucleation boiling governed heat transfer mechanism while at high thermal loads, forced convective boiling which is linked with thin film evaporation contributed greatly to thermal transfer. Hung et al. [65] numerically investigated the effects of channel outlets enlargement (Fig. 19) on thermodynamic performance of porous MCHS. It was determined that although a pressure drop was accompanied by a higher Nusselt number, it could be mitigated by raising either the width enlargement ratio or height enlargement ratio of the channel output. Also, the heat transfer effectiveness increased with the increase of the ratio, for the same pumping power. Lu et al. [66] studied ways to incorporate wavy and porous designs (Fig. 20) into one to lower drop in pressure and reduce thermal resistance simultaneously. Pressure drop decrease was attributed to a combined effect of permeation and slip effects of the fluid. Heat transfer enhancement was credited to enhanced mixing due to Dean vortices, elongated flow route due to increase in equivalent channel length and forced permeation due to impingement.

SN	Reference	Enhancement	Solution Method	Dimensions	Working Fluid	Operating parameters	Enhancement Effect
1	Sarafan et al. [56]	porous MCHS	Num.	H = 400 μm	Non-Newtonian power law	$q_1 = 1150$ W/m^2 $q_2 = 50$ W/m^2 $T_{w,in} = 314.231$ K $u_{in} = 0.1455$ m/s	
2	Li et al. [57]	porous MCHS	Num.	W = 0.5 mm H = 1 mm	Water	$p_{out} = 0$ Pa $q_w = 100$ W/cm^2 $T_{in} = 300$ K	When the solid ribs are replaced by porous ribs, the pressure drops for the middle, symmetrical and staggered ribs reduce about 67%, 57% and 12%, respectively The non-uniform velocity in the porous region intensifies the fluid mixing, which disturbs and redevelops the thermal boundary layers and facilitates the convective heat transfer

SN	Reference	Enhancement	Solution Method	Dimensions	Working Fluid	Operating parameters	Enhancement Effect
3	Dehghan et al. [58]	porous MCHS	Ana.		clear-fluid flow		Using a rarefied porous insert was found to effectively enhance the HTP of a heat exchanger
4	Dehghan et al. [59]	porous MCHS	Comb: Ana. & Num.		clear-fluid flow		Local Nusselt number decreases with increased temperature jump coefficient (β), with increased internal heat generation parameter (ωs), and with decreased effective conductivity ratio (k)
5	Haddad et al. [60]	vertical open-ended microchannel filled with porous media	Num.		Newtonian fluid		The friction factor is found to decrease as Knudsen number, Forchheimer number and Grashof number are increased
6	Jia et al. [61]	porous-wall MCHS	Expt.	W = 150 µm H = 80 µm	acetone	G = 255, 428, 614, 843 kg/m^{2}s q = 4 – 110 W/cm^2 x_{exit} = 0 – 0.88	The CHF of PW microchannels increases with mass flux and compared to Rec microchannels, the PW microchannels delay the premature dryout and increase the CHF because of the wicking effects introduced by pin fins arrangement to maintain the liquid rewetting
7	Mondal and De [62]	porous microchannel for non-Newtonian fluid with electrokinetic effects	Ana.		non-Newtonian fluids		For EOF assisting the pressure-driven flow, Sherwood number could be enhanced to more than five times for h > 30, compared to an impervious conduit.
8	Zargartalebi et al. [63]	Partially porous MCHS	Num.	Pr = 1, L* = 32, H* = 16, D^*_{pin} = 1, l* = 1, h* = 1, L^*_p = 8 and L*1 = 4, t* = 40 for transient conditions	Newtonian fluid		As the height of the porous media reduced, the flow through the medium was by-passed, more so in the staggered pin-fin configuration than the inline
9	Hung et al. [67]	Porous-MCHS with Different Porous Configurations	Num.			U_{in} = 0.2 to 6 m/s Re = 45 ~ 1350 T_{in} = 293 K No slip conditions	MCHS with sandwich distribution has the smallest increment in friction factor (and thus lowest pumping power requirements) while the one with rectangular porous distribution has the greatest one
10	Deng et al. [64]	Porous MCHS with reentrant microchannels	Expt.	W = 0.4 mm H = 1.1 mm D = 0.8 mm Depth of re-entrant cavity = 0.3 mm $D_{h,\ Reentrant\ porous\ MCHS}$ = 0.786 mm $D_{h,\ Reentrant\ copper\ MCHS}$ = 0.781 mm	Water	G =125 – 300 kg/m^{2}s T_{in} = 33 °C, 60 °C and 90 °C	Comparisons with Reentrant copper MCHS showed a significant wall superheat indicating lower thermal impedance, lower boiling instabilities, and a 100%-400% increase in HTC

2.6 Nanostructures

As seen in prior examples, an increase in surface area has corresponded to a rise in the HTC observed. Nanostructures offer a wide variety of unique properties; large specific area, high thermal conductivity, wettability manipulation etc [9, 68].

Ghosh et al. [69] used facile fabrication method to manufacture nanostructures on microchannels to improve flow boiling heat transfer. Sharp needle like superhydrophobic nanostructures of CuO were formed on surface of microstructures using a simplistic and self-regulating chemical oxidation technique. Like in previously discussed studies,

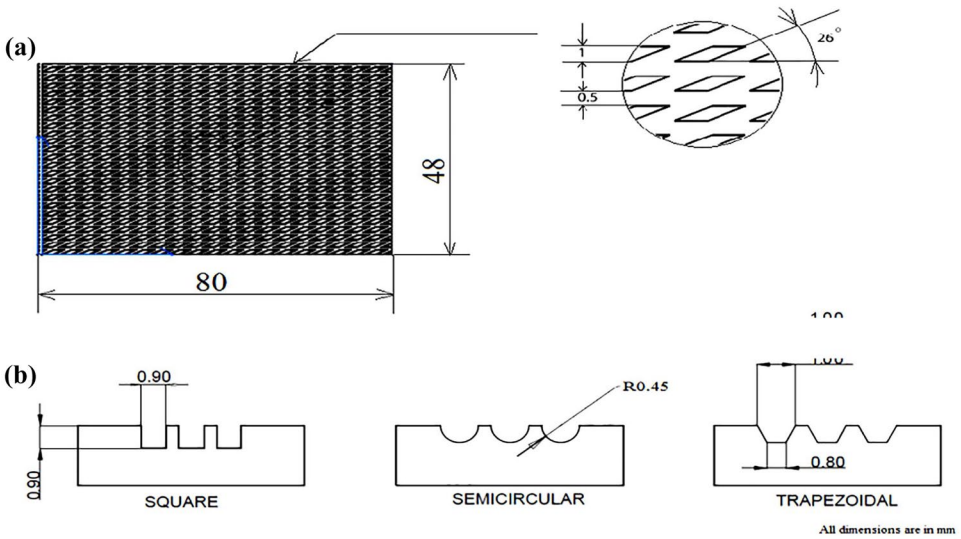

Fig. 15 (**a**) Oblique finned MCHS (**b**) Various cross-sections of channel of oblique finned MCHS [49]

the authors found an appreciable increase in performance of heat transfer, with a reduced pressure drop as well as reduced average amplitude of fluctuations as compared to PW-MCHS. Existence of a capillarity-fed thin-film evaporation regime in NSM was determined which as well was not detected in the case of PW-MCHS. Nagayama et al. [70] investigated the applications of surfaces with nanostructure in parallel-(SS) plate microchannel for augmentation of thermal dissipation. Four cases (Fig. 21) were examined; Ni nanostructure plated SS, Ni-St nanostructure plated SS, Ni-St and alumina plated SS and $FeCl_3$ and fluoride etched SS. Nanostructures of 1μm layer thickness of approximately 50 nm are produced amongst the microscale structures that ranged from 1000 nm to 3000 nm. The larger contact angle (Fig. 22) was found for case 1, as compared to the bare surface, while the surface hydrophility was found to be improved for the other cases. The hydrophilic nanostructured surfaces obtained higher HTC.

Alam et al. [71] researched to determine the flow boiling characteristics in Silicon Nanowire (SiNW) MCHS while comparing it's performance to rec-MCHS using HFE-7100 as coolant. The SiNW MCHS showed higher effective wall flux for the wall superheat, higher effective HTC, and lower drop in pressure (ergo lower pumping power) for same vapour quality, higher heat transfer (up to 400%) and lesser boiling instability (up to 70%) over a variety of mass flux rates. Flow visualization captured using high speed cameras (Fig. 23) showed that explosive bubble nucleation rather than discrete bubble nucleation was experienced in SiNW MCHS. Explosive boiling was followed by vapour bubbles coalescing to form annular flow.

Yang et al. [72] studied the use of Nanowire-Coated Microchannels for the heat transfer enhancement during flow boiling using HFE-7000 as coolant. Enhancement of HTC of up to 344% along with a decline in required pumping power by 40% was observed. CHF was enhanced by 14.9% at mass flow rate of 1018 kg/m^2•s was observed. However, the trend observed in CHF was non-monotonic and value reduced at elevated mass flux.

SN	Reference	Enhancement	Solution Method	Dimensions	Working Fluid	Operating parameters	Enhancement Effect
1	Ding et al. [73]	CuO nano-structures	Expt.	D_h = 0.67 mm	R141b	G = 70 - 850 Kg/m^2s	Increase in contact angle positively influenced the HTC
2	Sharma et al. [74]	CuO nano-structures	Expt.	W = 300 μm H = 500 μm	Water	G = 354 ±25 Kg/m^2s q = 8 ±5 - 220 ± 5 W/cm^2	N-MCHS gave better heat transfer performance than PW-MCHS. Rewetting flow was also improved with liquid front velocity being almost twice as fast.
3	Ghosh et al. [69]	CuO nano-structures	Expt.	W = 500 μm H = 250 μm	DI water	Q = 20 - 50 W G = 362 kg/m^2s	Increase in performance of heat transfer, with a reduced pressure drop as well as reduced average amplitude of fluctuations as compared to PW-MCHS

SN	Reference	Enhancement	Solution Method	Dimensions	Working Fluid	Operating parameters	Enhancement Effect
4	Hedau et al. [75]	CuO nanostructures	Expt.	W = 315 ± 15 µm H = 600 ± 10 µm	DI water	q = 23 - 220 W/cm^2	Surface temperature (1–2.5 °C), maximum heat flux and fluctuations was found to be the lowest in NSW with inlet restrictors and the highest in PW MCHS.
5	Hendricks et al. [76]	ZnO nanostructures	Expt.	Area = 9.1 cm^2	DI water		Heat transfer coefficient recorded was improved by a factor of 10 and CHF by a factor of 4 as compared to plain aluminium substrate.
6	Gao et al. [77]	Nickel nanostructures	Expt.	Area = 50 x 50 mm^2 Nanostructure area = 20 × 20 mm^2	DI water	q = 3.5 - 47.5 W/cm^2	As compared to plain microstructures and more so as compared to smooth surfaces, the nanostructure boosted the amount of nucleation sites available by lowering the energy barrier of phase change. The HTC was significantly higher
7	Alam et al. [71]	Silicon Nanowire (SiNW) microchannels	Expt.	W = 220 µm H = 250 µm SiNW Dia. = 20 nm length = 5 µm	HFE-7100	G = 400–1600 Kg/m^{2}s	The SiNW MCHS showed higher effective wall flux for the wall superheat, higher effective HTC, and lower drop in pressure
8	Yang et al. [72]	Silicon Nanowire (SiNW) microchannels	Expt.	W = 220 ± 2 µm H = 250 ± 5 µm SiNW Dia. = 20 - 100 nm length = 5 µm	HFE-7000		Enhancement of HTC of up to 344% along with a decline in required pumping power by 40% was observed. CHF was enhanced by 14.9% at mass flow rate of 1018 Kg/m^{2}s was observed.
9	Yao et al. [78]	Silicon Nanowire (SiNW) microchannels	Expt.	W = 100 - 300 µm H = 150 µm Area = 10 x 10 mm silicon chip **SiNW** Top/bottom surfaces: d = 10 – 50 nm, l = 10 – 20 µm Side wall: d = 80 - 100 nm, l = 10 µm	DI water	q = 10 - 160 W/cm^2	Maximum heat flux was enhanced by 120% as compared to MCHS.

3 Solution approaches

On the path to determine the performance of microchannels, researchers have opted for many different techniques often in conjunction with each other to arrive at their conclusions. The three main techniques used have been experimental, analytical & numerical. Experimental techniques utilize a physical setup with the equipment running at the target conditions. Several parameters need to be taken into consideration simultaneously to avoid a deviation from expected results. Inaccuracies in setup, as well as measurement have to be factored in. Also, there is a need to repeat the experiment to prevent any transients from causing deviations. Analytical studies require solving of theoretical equations with the requisite initial as well as boundary conditions (and assumptions if any) to arrive at a solution. Numerical methods utilize different numerical methods which are utilized to solve the theoretical equations with initial and

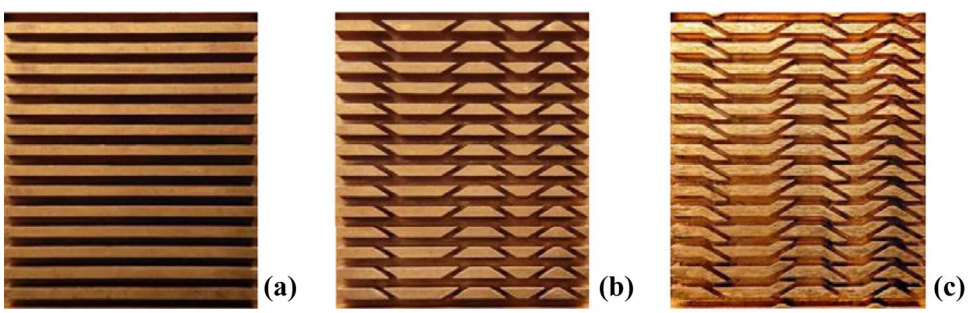

Fig. 16 (**a**) RS-MC (**b**) AOT-MC (**c**) AOTF-MC [52]

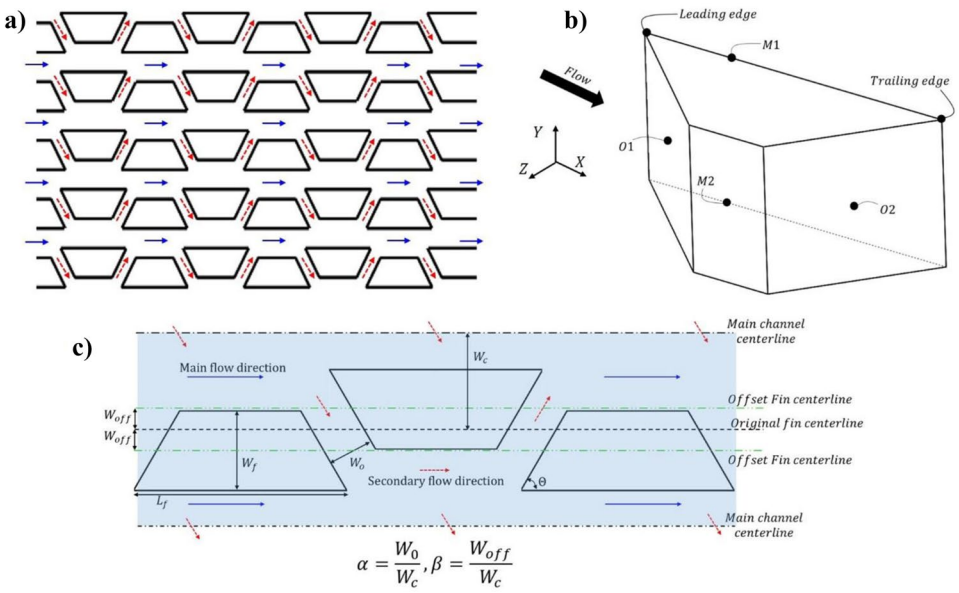

Fig. 17 (**a**) Planar view of AOOMC showing periodically discontinuous offset fins, (**b**) fin nomenclature, and (**c**) critical geometric parameters of AOOMC [53]

boundary conditions applied. The numerical methods, if employed have to be validated initially with relevant experimental data if it is going to be used to be used for simulation of unknown conditions.

In the paper we are going to examine some of the experimental setups used and advantages and challenges in each, analytical as well as numerical techniques utilized.

3.1 Experimental

In experimental methods, the microchannels are setup with a known and a predictable thermal load being supplied. Coolant is supplied at a known rate across the microchannel and temperature at the inlet and outlets measured. Depending upon the experimental requirements, the load can be varied, and the effects measured. A setup used by Mathew et al. [15] is shown in (Fig. 24). The schematic represents the general setup which is used in many research studies albeit with a few differences. The pump, usually a positive displacement type pumps the fluid through a heat exchanger to the test section. A by-pass or pressure relief valve placed after the pump is used to discharge the fluid back to the reservoir in case of over pressure or emergency shut down or even to adjust the system flow rate [79]. The heat exchanger maintains the passing fluid at a pre-set temperature. It is physically located as close to the test section as well as (*usually*) positioned after the pump to reduce the possibility of heat influx into the fluid due to increased piping requirements and to ensure that work input by pump does not alter the fluid temperature. The test section is supplied with a predefined and constant thermal load usually with the help of resistance heating coils. A power supply unit is used to energize the coils and maintain a constant load. The fluid after passing through the test section is sent to a reservoir via an air-cooled condenser. The condenser is substituted by a heat exchanger if the fluid exiting the test section has not undergone phase change. In several experimental studies, the phase change/ bubble formation/ flow studies in the test section need to

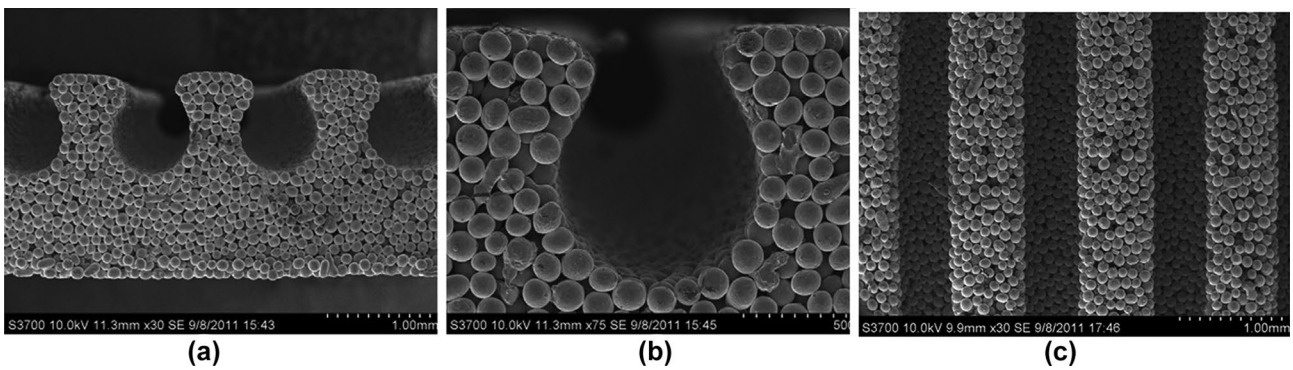

Fig. 18 SEM imagery of re-entrant porous MCHS: (**a**) MCHS cross section (**b**) Single re-entrant MCHS cross section (**c**) MCHS top view [64]

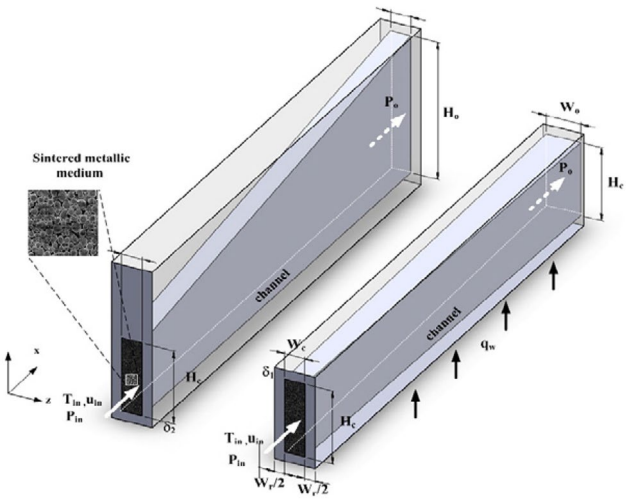

Fig. 19 Diagram of porous MCHS and computational domain [65]

be studied. To facilitate the same, the test section is usually covered by a transparent acrylic top cover and a camera (usually high speed) is fitted overhead to capture the flow. A data acquisition system (DAQ) is typically utilized to capture the different parameters (pressure, temperature, flow rate etc.) that are required. Pressure transducers, temperature probes, flow meters etc. are used to capture the pressure, temperature, and flow data.

Several variations of the above setup exist depending upon the requirements of the experiment. Gear pumps [15, 80] are used quite often used. Other types of pumps that may be used are HPLC [81], peristaltic [82], volumetric [83] etc. Target flow rates are usually 5 g/s - 35 g/s and are varied using a flow control valve and monitored using a rotameter/flowmeter. A filter is generally used after the pump to prevent contaminants being driven to the test section.

Temperature monitoring is usually done using thermocouples. J-, K- & T- type thermocouples are often used. Each of the thermocouples utilized have a particular temperature range as well as an accuracy. Selection is done after analysing the approximate temperatures expected and knowing the required accuracy. The Table 1 [84] gives an indication of how the operating temperature limits and the uncertainty of measurement of each thermocouple type. Thermocouples are usually embedded within the test piece in holes drilled for the purpose (Figs. 25 and 26).

Pressure measurement has been done absolute and differential pressure transducers [82]. Thermocouples and pressure transducers are coupled to a standalone data acquisition (DAQ) system which is able to read data from the thermocouple and record data to internal or external data storage unit against a time domain. Some researchers [81] use a dedicated DAQ while others use a data logger (like NI) [82] which can be interfaced to (and controlled from) a computer.

The test section houses the test piece (microchannel), a source of known heat flux and the requisite sensors measuring the performance of the MCHS. The microchannels are generally embedded within a Teflon or acrylic block which are shaped to directs flow through the MCHS while simultaneously reducing leakage heat flux to the surroundings. The inlet and outlet channels, also known as plenum, also house the pressure transducers. The top cover (e.g., Fig. 25) can be made of a transparent plexiglass which will allow observation and recording of the experimentation using a camera. It must be ensured that leakage around the MCHS does not occur. Heat flux is provided using cartridge heaters, strip heaters, plate heaters [75, 82, 85, 86] etc. Power to the heater is regulated and monitored carefully to ensure accurate thermal flux input to the test section.

Following the recording of experimental data, the data needs to be post processed to be converted to a relevant form. Parameters such as heat transfer coefficient can be calculated.

$$h_{\mathrm{exp}} = \frac{q_{\mathrm{app}} f_{\mathrm{eff}}}{A_{\mathrm{d}}\left(T_{\mathrm{S}} - T_{\mathrm{f\_in}}\right)} \tag{2}$$

where q_{app} is the applied device power, A_d is the footprint area of the device, T_{f_in} is the measured temperature of the coolant at inlet, and T_s is the local surface temperature of the

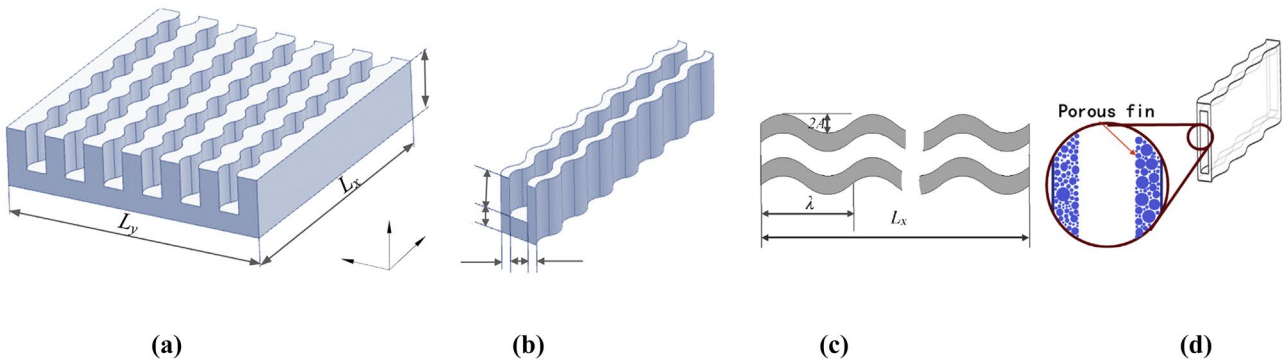

Fig. 20 (**a**) Wavy MCHS; (**b**) periodic unit (simulation domain); (**c**) wavy length and magnitude; (**d**) porous finned MCHS [66]

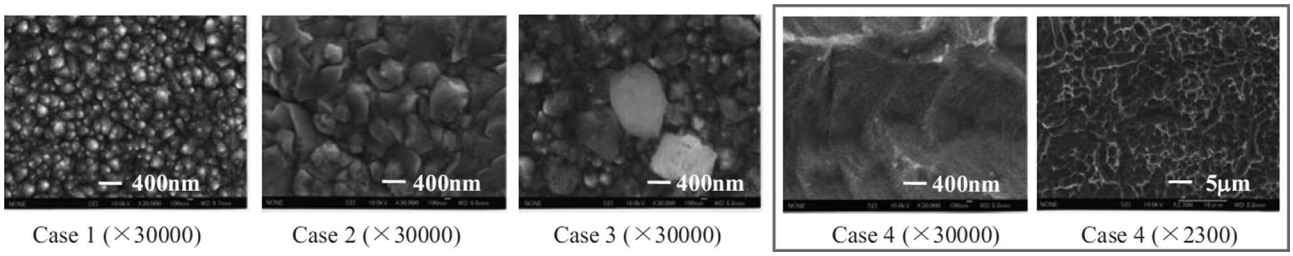

Fig. 21 SEM imagery of the SS plates with nanostructures [70]

cold plate below the heater thermocouple [87]. Parameters such as thermal resistance, Reynolds, Prandtl and Nusselt numbers can also be calculated. Factoring the least count of each of the instruments, error analysis/ uncertainty needs to be factored in.

Hedau et al. [86] experimentally (and numerically) determined the impact of variation of number of parallel microchannels on thermal dissipation during flow boiling. It was observed that vapour bocking the outlet was the primary source for oscillations and instabilities in the drop in pressure. A reduction in surface temperature by 45.5 °C, a rise in pressure drop by 37% as well as a rise in HTC by 240% was observed when there was a change in the number of channels from 6 to 14. The local temperature of the chip and local Nusselt numbers can be measured with the help of a high-resolution IR-range Imaging. Kadam et al. [88] investigated single-phase heat transfer in MCHS and their performance augmentation. Two configurations of the open MCHS were manufactured and analyzed: the plain open MCHS and the extended open MCHS, with the later providing superior thermal performance, a 9% improvement in heat flux and an 18% improvement in HTC albeit with an 18% greater drop in pressure.

Markal et al. [89] researched flow boiling in Rec-MCHS (with square cross section) and the influence of hydraulic diameter on it. Effects of mass and heat flux, and vapor quality on the thermal dissipation and total pressure drop were studied and it was found that hydraulic diameter had a substantial impact on both of the local two-phase HTC and the overall pressure drop. Yang et al. [90] conducted performance evaluation of with regards to thermal dissipation observed in single-phase array pin fin MCHS with different configurations (Triangular, square, pentagonal, hexagonal and circular cross sections). The pin fin shapes were found to impact drop in pressure and rate of thermal dissipation for attaining improved cooling performances of the single-phase array MCHS. Peles et al. [91] investigated forced convection in pin fin MCHS. It was determined that large amounts of heat flux can be dissipated with a reduced wall temperature compared to plain walled MCHS. HTC for micro-scaled pin-fins were found to be very high.

3.2 Analytical

Analytical solutions are mathematical solutions to mathematical expressions with stated boundary and initial conditions. The advantages of analytical solutions are two-fold; one of transparency, with the solution presented to math expressions modelled after the physical phenomenon, offering a strong and unambiguous understanding into how different parameters and variables and interactions between the variables themselves alter the outcome. The other advantage is efficiency. Algorithms and models conveyed with analytical solutions are quite often more efficiently expressed than using equivalent numerical models/techniques. E.g., for solutions of ordinary differential equations, analytical methods will arrive at a much more accurate solution quicker as compared to numerical techniques [92]. Equations used to arrive at analytical solutions however form the basis for numerical methods.

In the field of microchannel fluidics, analytical solution techniques have not been widely used due to the

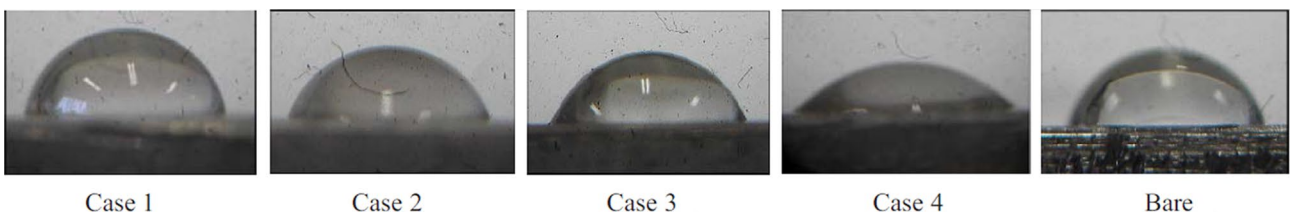

Fig. 22 Contact angles of water droplets on various surface structured SS plate [70]

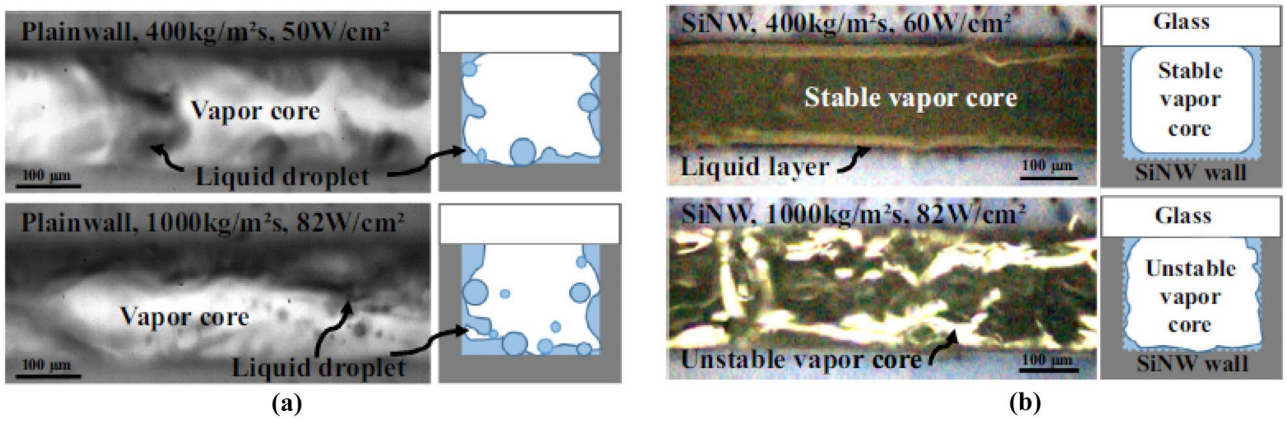

Fig. 23 Annular flow patterns at various heat and mass fluxes between (**a**) Plain wall and (**b**) SiNW MCHS [71]

complexity of the equations and the types of flow and flow conditions experienced. There are however a few notable examples. M. Dehghan et al. [59] conducted an analytical investigation examining forced convection across the entrance zone of a MCHS filled with porous material (Fig. 27). Energy conservation equation within solid and fluid phases of the porous materials was taken into account (3) [59]. Assumption of high Peclet number was taken.

$$\begin{aligned} \rho c_p u \frac{\partial T_f}{\partial x^*} &= k_{f,\,\mathrm{eff}} \frac{\partial^2 T_f}{\partial y^{*2}} + h_{sf} a_{sf} \left(T_s - T_f\right) + S_f, \\ 0 &= k_{s,\,\mathrm{eff}} \frac{\partial^2 T_s}{\partial y^{*2}} - h_{sf} a_{sf} \left(T_s - T_f\right) + S_s. \end{aligned} \tag{3}$$

Here, ρ is fluid density (kg.m^{-3}), c_p is specific heat at constant pressure (J.kg^{-1}.K^{-1}), u is Darcian velocity (m.s^{-1}), T_f is Temperature of fluid phase (K), $k_{f,\,\mathrm{eff}}$ is effective thermal conductivity of the fluid phase (W.m^{-1}.K^{-1}), x^* and y^* are dimensional coordinates (m), h_{sf} is fluid-solid heat transfer coefficient (W.m^{-2}.K^{-1}), a_{sf} is specific surface area (m^{-1}).

The equation was converted into parametric form (4) to yield an exact solution in the form of (5) [59].

$$\left(\theta_s - \theta_f\right) = \Delta NE = \frac{1}{Bi}\frac{\partial^2 \theta_f}{\partial y^2} + \frac{1}{Bi}\omega_s + O\left(Bi^{-2}\right) \tag{4}$$

$$\begin{aligned} \theta(\mathrm{x},\mathrm{y}) = &\frac{\left(\omega_\mathrm{s} + \omega_\mathrm{f} + 1\right)}{\mathrm{k}}\mathrm{x} + \frac{3(\mathrm{y}-1)^2 - 1}{6(\mathrm{k}+1)} \\ &- \sum_{\mathrm{n}=1}^{\infty}\left[\frac{2}{\mathrm{k}\sigma_\mathrm{n}} exp\left(-\sigma_\mathrm{n}\mathrm{x}\right) cos(\mathrm{n}\pi\mathrm{y})\right] \end{aligned} \tag{5}$$

Here θ_s and θ_f is dimensionless temperature of solid and fluid respectively, ΔNE is LTNE intensity, Bi is Biott

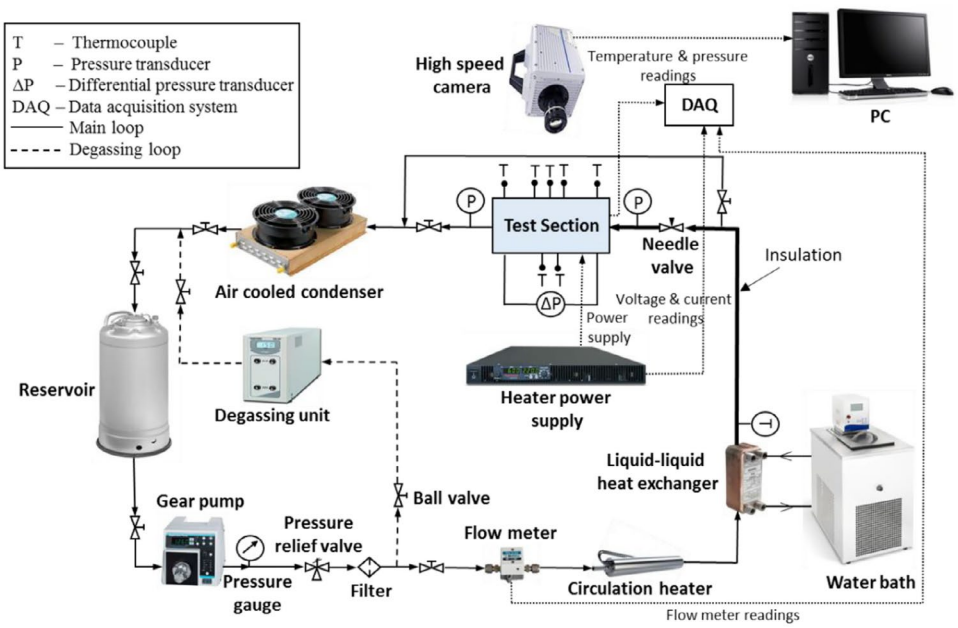

Fig. 24 Schematic of experimental flow loop [15]

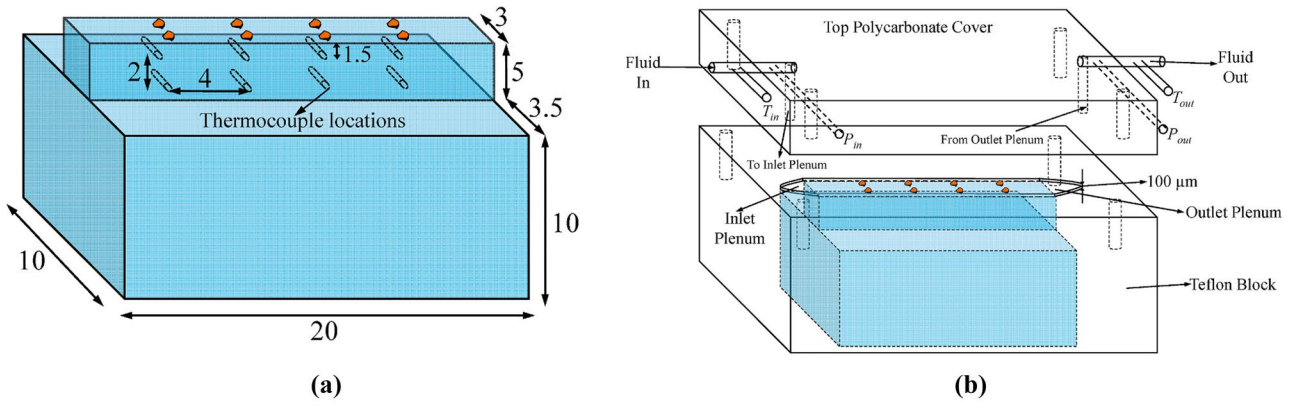

Fig. 25 (**a**) Copper test block (all dimensions are in mm), and (**b**) exploded view of the test section [82]

Number, x, y are dimensionless coordinates, half of the channel gap (m), $k_{s,\text{eff}}$ is effective thermal conductivity of the fluid phase ($\text{W.m}^{-1}\text{.K}^{-1}$),

$$\theta = \frac{(\text{T} - T_i)k_{s,\text{eff}}}{q''_w H}, x = \frac{x^* k_f}{\rho c_p H^2 u} = \frac{{}^{x^*}/_H}{Pe}, y = \frac{y^*}{H},$$

$$k = \frac{k_{f,\text{eff}}}{k_{s,\text{eff}}}, \omega = \frac{SH}{q''_w}, Bi = \frac{h_{sf} a_{sf} H^2}{k_{s,\text{eff}}}$$

Equation and corresponding solution for Nusselt number were also determined. Pavuluri et al. [93] while developing a numerical solution looked at arriving at an analytical solution for spontaneous imbibition in a rectangular MCHS. Starting with the Hagen–Poiseuille equation for average velocity, they arrived at the equations for dimensionless velocity (6) and time (7) [93, 94].

$$U^* = \frac{U_\text{m}}{U_\text{ref}} = \frac{6hU_\text{m}\mu_n\updownarrow}{\left(h^2 + 6h\lambda + 6\lambda^2\right)\sigma\cos(\theta)} \tag{6}$$

$$t^* = \frac{t}{t_\text{ref}} = \frac{\left(h^2 + 6h\lambda + 6\lambda^2\right)\sigma\cos(\theta)t}{6h\mu_n\updownarrow^2} \tag{7}$$

U^* is dimensionless velocity, U_m is meniscus velocity, U_ref is reference velocity, t^* is dimensionless time, h is Height of the channel, λ is Slip length (m), σ is Surface tension between fluids (kg/s^2), θ is equilibrium contact angle, t is time. Numerical solutions agreed with the analytical results.

3.3 Numerical

Numerical techniques are used to study the bounds of validity of analytical solutions and extend research into time (and or other variable) dependant problem numerical solution is obtained. Dey et al. [95] explored the impact of varying gravity conditions on the characteristics of thermal dissipation of R134a in MCHS. The general process followed in numerical computation is given below [96]:

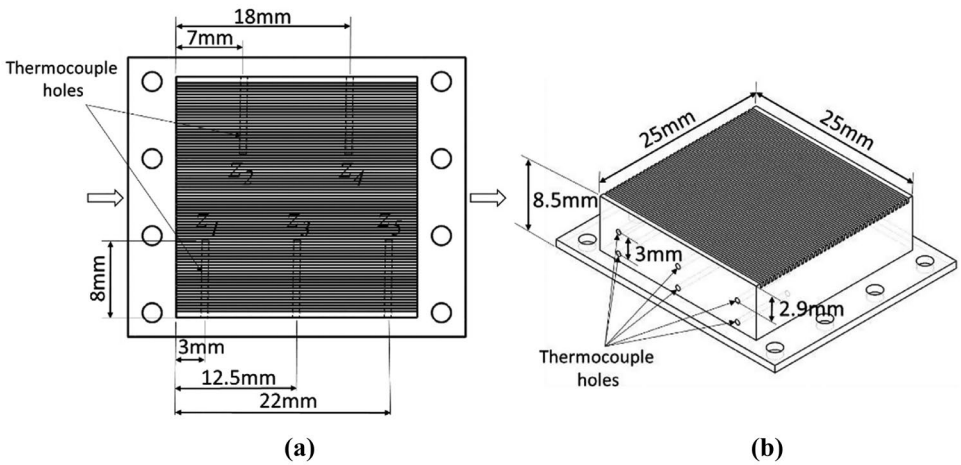

Fig. 26 Copper heat sink with indications for the thermocouple hole locations (**a**) Top view and (**b**) isometric views [15]

Table 1 Thermocouple temperature measurement range and uncertainty [84]

Thermocouple type	Temperature Range	Uncertainty
S	0-1600 °C	±1 °C up to 1100 °C ±0.003×(T-767) °C >1100°C
R	0-1600 °C	±1 up to 1100 °C ±0.003×(T-767) >1100 °C
B	200-1700 °C	±0.0025×(T-767) 600-1700 °C
E	0-800 °C	±1.5 °C
J	0-760 °C	±1.5 °C
K	0-1100 °C	±1.5 °C
N	0-1100 °C	±1.5 °C
T	-185-400 °C	±0.5 °C

1. Creation of a mathematical model.
2. Formation of an applicable numerical method.
3. Execution of the method to find a solution.
4. Solution validation.

Abiev [97] used CFD calculations for slug flow in MCHS to determine bubble velocity, Taylor circulation and mass transfer model. Bordbar et al. [98] looked to understand application of numerical simulations in studies of slug flow in MCHS. Jang and Choi [99] looked to determine the performance with respect to cooling of nanofluids (6 nm Cu-H_2O and 2 nm diamond- H_2O) in MCHS. Results showed that performance with respect to cooling had an enhancement of approximately 10% in comparison to that of a MCHS with water. Nanofluids decrease both the thermal resistance as well as the variation in temperature difference between the coolant and the microchannel wall with heat flux.

Kuppusamy et al. [100] examined the enhancement of thermodynamic characteristics of MCHS with secondary flows. The secondary flows caused the regeneration of the hydrodynamic and thermal boundary layer thus resulting in lower thermal resistance (reduced by 76.8%) and greater heat transfer performance (increased by 146%) albeit with some pressure penalty (up to 6%). Kuppusamy et al. [101] also investigated trapezoidal grooved microchannel heat sink (TGMCHS) utilizing nanofluids studying the thermal and fluid flow fields. Results show that TGMCHS have a superior performance as compared to rec-MCHS.

Shen et al. [102] conducted thermal performance studies numerically on staggered flow alternation structure (SFAS) equipped Double-layer Microchannel Heat Sinks (DL-MCHSs) (Fig. 28). Best position of SFAS with respect to thermal performance in the DL-MCHSs was observed to be on the basis on different locations and multi-flow directions and it had the advantage of not having an appreciable pressure drop penalty.

Leng et al. [103] conducted optimization studies on double-layered MCHS (DL-MCHS) considering their thermal resistance and bottom wall temperature. Channel width, channel number, bottom channel height, and bottom coolant inlet velocity were the search variables used for attaining optimization of heat sink performance. Wu et al. [104] conducted parametric performance analysis on Double-Layered MCHS (DL-MCHS) while comparing them to single layered MCHS (SL-MCHS). With taller aspect ratio (lower microchannel breadth) and larger channel number (small width ratio), DL-MCHS were found to be better able to handle conditions where higher pumping power was provided. Xia et al. [105] investigated numerically fan-shaped re-entrant cavities and internal ribs equipped (FRCR) MCHS (Fig. 29) with regards to their thermal performance. Friction factor of the FRCR for $e/D_h > 0$, was determined to be 1.2-6.5 times greater

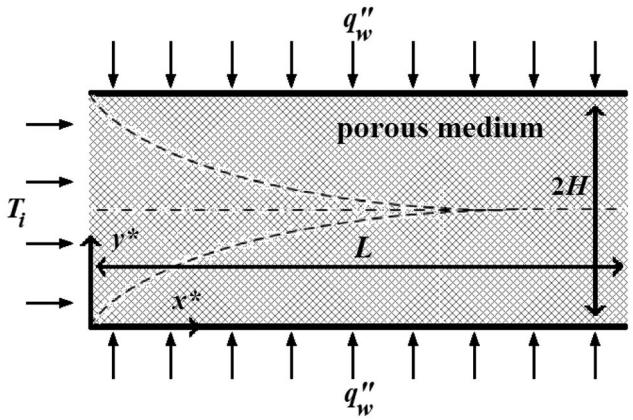

Fig. 27 Schematic diagram of the problem [59]

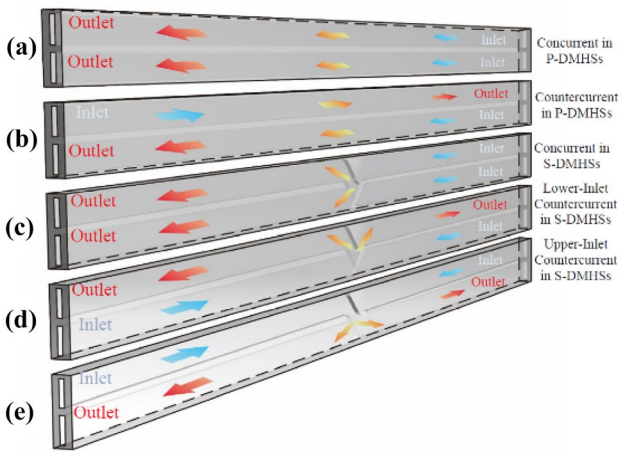

Fig. 28 Detailed schematic diagram of different working flow directions for P-DL-MCHS (P-DMHS): (**a**) concurrent (**b**) counter current and for S-DLMCHS (S-DMHS) (**c**) concurrent flow (**d**) lower-inlet counter current (**e**) upper-inlet counter current [102]

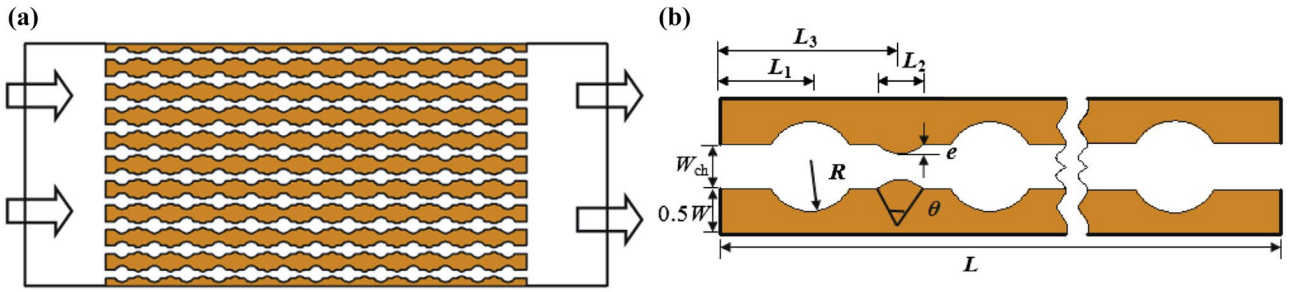

Fig. 29 (**a**) Structure of a parallel MCHS and (**b**) the numerical domain [105]

values determined for the rectangular MCHS, however the observed Nusselt number of FRCR was found to be 167% more and having a dependence on the Reynolds number (Fig. 30).

Szczukiewicz et al. [106] worked on numerical simulations of two-phase boiling in MCHS. The authors modelled and highlighted the significance of the thermal inertia of the liquid film trapped between vapour slugs and the wall and flow recirculation in the liquid between two bubbles on the determination of HTC.

4 Microchannels with single and multi phase flow

4.1 Single phase

Single phase cooling solutions utilize the fluids' sensible heat capacity to provide cooling in the MCHS.

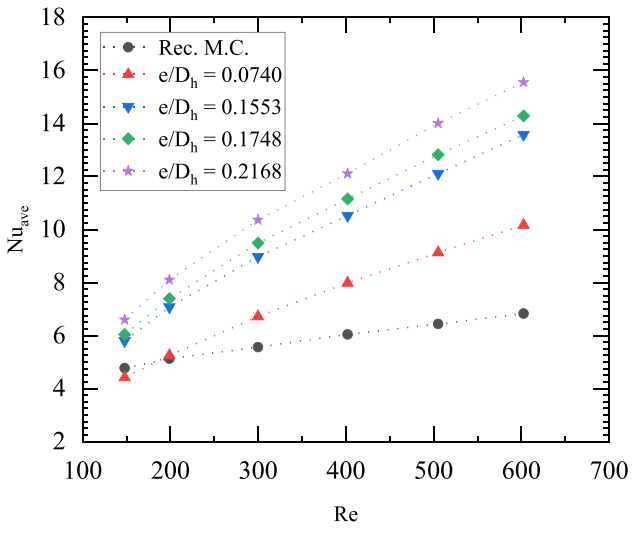

Fig. 30 Nuave vs Re for various rib heights [105]

Yang et al. [107] investigated the cooling of hybrid MCHS with a combination of manifold with secondary oblique channels (MMC-SOC) using HFE-7100 in single phase. The outcomes indicated MMC-SOC heat sinks could concurrently decrease the thermal resistance (by 24%) and drop in pressure (by 11%) in comparison to conventional manifold microchannel (MMC) heat sink. Arie et al. [108] performed modelling using numerical techniques and optimization of thermal performance of a single-phase flow MMC plate heat exchanger (Figs. 31 and 32).

Evaluating the performance of the optimized MMC with a chevron-type plate heat exchanger, (a commonly used plate heat exchangers) indicated that the MMC for three differing chevron angles had a better performance in terms of Nusselt number and friction factor.

Chauhan et al. [109] investigated the use of single-phase MCHS cooling for hotspot mitigation on microprocessors. To compare the baseline design for a typical microprocessor to an optimized device, a computational model was developed. Dede [110] investigated the use of single-phase microchannel cold plate (Fig. 33) for thermal management in hybrid vehicle electronics. A favourable thermal-fluid performance was observed in the multi-pass branching microchannel cold plate.

Oudah et al. [112] researched the impact of hybrid sandblasted patterns on single-phase MCHS considering their heat transfer performance. The modified surface with hybrid micro-sandblasting of elliptical patterns (HSEP) was found to improve the thermal dissipation performance considerably in comparison to the performance observed with the bare surface (BS) microchannel. Fully sandblasting (FS) lower surface of the MCHS however, enhanced the thermal dissipation performance only marginally. The drop in pressure observed in the HSEP was seen to increase slightly in comparison to the FS and BS. Sahar et al. [113, 114] examined the thermal dissipation and pressure drop properties in single-phase rectangular MCHS with various

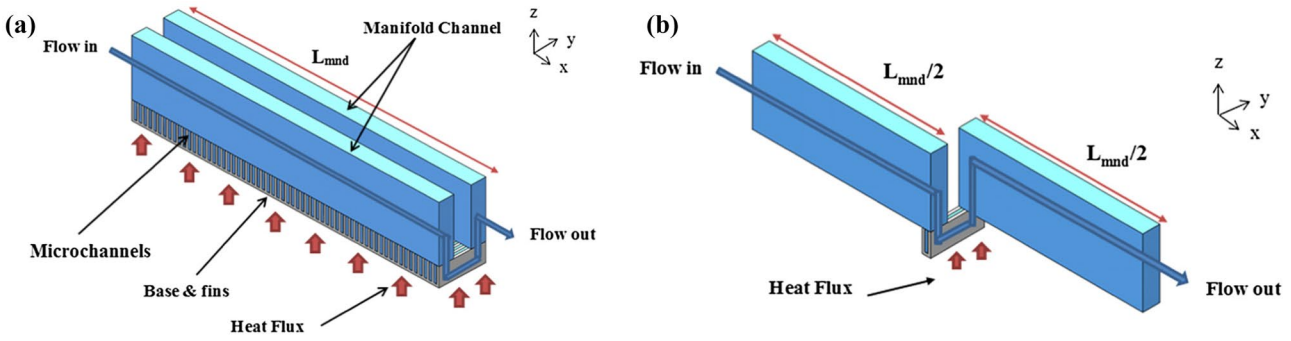

Fig. 31 (**a**) Single pass and single manifold (SPSM), (**b**) Single MMC [108]

configurations. In the single channel configuration (hydraulic diameter of 561 µm); four models were numerical examined; 2-D and 3-D thin-wall (heat flux applied from the bottom), 3-D thin-wall (heating on three side) and 3-D full conjugate models. 3D full conjugate model was exclusively used in the multichannel configuration (25 channels, hydraulic diameter of 409 µm). The aspect ratio was found to not affect the HTC while the friction factor and the Nusselt number were found to increase with the increase in hydraulic diameter. Sharma et al. [115] investigated the thermo-fluidic and energetic properties of a manifold MCHS utilizing recovered hot water (from cooling hot components and intended to be used to cool hotter components) as working fluid. The large fluid flow rate and elevated fluid temperatures were determined to cause turbulent flow conditions in the manifolds (inlet and outlet) of the heat sink with primarily laminar flow conditions observed in MCHS. Entropy generation due to heat transfer was contributed greatly to the net entropy generation in the heat sink. Use of hot water was determined to reduce the heat transfer component of entropy generation meaningfully, resulting in greater 2nd law efficiency.

S.N.	Reference	Enhancement	Solution Method	Dimensions	Working Fluid	Operating parameters	Enhancement Effect
1	Yang et al. [107]	Hybrid MCHS with Comb. of manifold with secondary oblique channels	Expt.	W = 150 µm $H_{MMC-1/MMC-SOC-1}$ = 60 µm $H_{MMC-2/MMC-SOC-2}$ = 100 µm θ = 45° W_{in} = 700 µm W_{out} = 350 µm	HFE-7100	q = 20, 25, 30, 35 W/cm^2 Re = 278 - 905 Q_v =211 - 580 mL/min	Results showed MMC-SOC heat sinks could concurrently decrease the thermal resistance (by 24%) and drop in pressure (by 11%) in comparison to conventional manifold microchannel (MMC) heat sink.
2	Arie et al. [108]	single-phase flow manifold-microchannel plate heat exchanger	Num.	W_{in} = 300 – 2000 µm H_c = 100 – 1000 µm	Water	Re_{mnd} = 100 - 1000 Q_{tot} = 10 kW m_{tot} = 0.1 kg/s	Optimization was done for different conditions
3	Chauhan et al. [109]	single-phase microchannel cooling for microprocessors	Num.	W = 0.1 mm H = 0.2 mm	Water	P_{in} = 13.8 kPa Q = 89.66W	The new chips that showed performance penalties of 2%, 5%, 8%, 11%, and 37% showed $T_{hspot,\,max}$ of 74.2 °C, 67.6 °C, 67.6 °C, 67.7°C, and 69.1°C respectively.
4	Dede [110]	Single-phase microchannel cold plate	Expt.	H = 0.5 mm	50/50 ethylene-glycol/ water	Q_v = 0.5 - 2.5 L/min (0.5 L/min increment) Q = 41 - 49 W	Increases cold plate thermal - fluid performance

S.N.	Reference	Enhancement	Solution Method	Dimensions	Working Fluid	Operating parameters	Enhancement Effect
5	Lin et al. [111]	MCHS with various manifolds	Num.	W = 50 µm H = 200 µm W_{fin} = 50 µm	HFE7100/ Water	q = 100 W/cm^2 $V_{in,\ Z\text{- type MMCs}}$ = 1.14 m/s $V_{in,\ C\text{-type MMCs}}$ = 1.14 m/s $V_{in,\ H\text{-type MMCs}}$ = 0.57 m/s $V_{in,\ U\text{-type MMCs}}$ = 0.0577 m/s $V_{in,\ ZU\text{-type MMCs}}$ = 1.14 m/s $V_{in,\ HU\text{-type MMCs}}$ = 0.57 m/s T_{in} = 303.15 K (water, single phase) Courant number < 0.25	The HU- type MMC heat sinks and ZU-type MMC heat sinks were determined to be preferrable owing to lower observed thermal resistance (<2×10^{-2} m^{2}K/kW and drop in pressure below 0.5 kPa)
6	Sahar et al. [113]	Rectangular MCHS	Comb. Expt.& Num.	$W_{Single\ channel}$ = 0.3 mm $W_{Multi\text{-}channel}$ = 0.297 mm $H_{Single\ Channel}$ = 0.7 mm $H_{Multi\text{-}channel}$ = 0.697 mm $D_{h,\ Single\ channel}$ = 0.561 mm $D_{h,\ Multi\text{-}channel}$ = 0.409 mm	Single Channel= Water multi-Channel= R134a		The aspect ratio was found to not affect the HTC while the friction factor and the Nusselt number were found to increase with the increase in hydraulic diameter
7	Sharma et al. [115]	manifold MCHS	Num.	W = 159 µm H = 1473 µm	Water	Re_{in} = 2000 – 11000 q_v = 0.3–1.0 L/ min T_{in} = 30 – 60°C	The large fluid flow rate and elevated fluid temperatures were determined to cause turbulent flow conditions in the manifolds
8	Shkarah et al. [116]	Rectangular MCHS	Num.	W = 56, 55, 50 µm H = 320, 287, 302 µm	Water	q = 181, 277, 790 W/cm^2 Q_v = 4.7, 6.5, 8.6 cm^3/s	Graphene was found to be the most effective in reducing the thermal resistance
9	Zhang et al. [117]	Rectangular MCHS	Expt.	W = 0.21 mm H = 2 mm Aspect ratio = 9.5 chip size = 10 x 10 mm, 12 x 12 mm	DI water	Q = 40, 60, 85 W Q_v = 0.83 x 10^{-5} to 1.67 x 10^{-5} m^3/s	Analytical method was developed to predict the pressure drop and thermal resistance

4.2 Two-phase

A shift to two-phase cooling schemes was done to utilize the coolant sensible as well as latent heat capacities, which allow rejection of greater quantity of heat than that possible in single-phase schemes, while maintaining lower temperatures. The heat flux is generally maintained below critical heat flux (CHF) levels to provide optimal cooling.

Radwan et al. [118] investigated the use of flow boiling (two-phase) in Double layered-MCHS (parallel & counter flow) using Ethyl Alcohol and Novec-7000 as coolant for thermal management in concentrated photovoltaic systems. The effects of changing the coolant type, coolant flowrate, simulated solar light concentration ratio, and heat sink design on the solar cell temperature distribution were investigated experimentally. It was determined that the two-phase flow boiling considerably lowered the maximum temperature in the cells and attained a much more consistent temperature distribution within the solar cell. It was also found to improve electrical efficiency. However, the parallel flow configuration was found to attain effective cooling only at higher flow rates in comparison to the counter flow

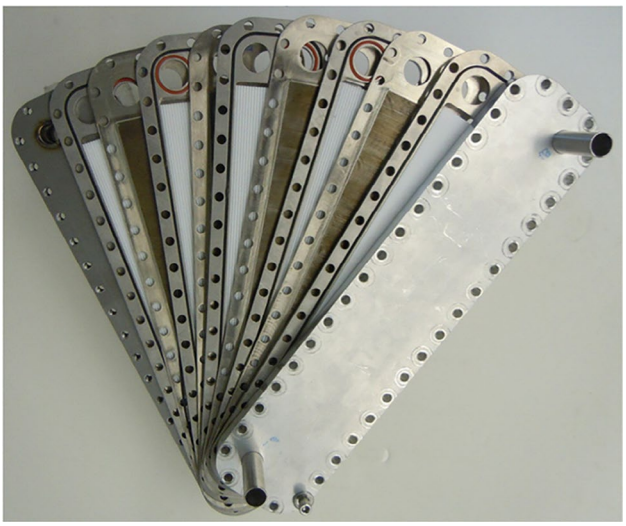

Fig. 32 Stacked manifold-microchannel plate heat exchanger [108]

configuration. In parallel flow, the use of ethanol as coolant resulted in higher efficiency at higher flow rates. However, in counter flow, the Novec-7000 results in higher efficiency values at all flow rates. Pourfattah et al. [119] performed analysis of the thermal characteristics of a manifold MCHS with H_2O/CuO nanofluid flow (Fig. 34) using two phase simulation. The results obtained showed the HTC and friction coefficient was improved by raising the in/out ratio at a steady Reynolds number. Also, there is substantially greater impact of in/out ratio at higher values of Re. The highest value of performance evaluation criterion was achieved with an in/out ratio of 0.25 and at the Re of 100 and solid concentration 2 vol%.

Chinnov et al. [120] studied the flow patterns for Two-phase flow in horizontal rectangular microchannels with the height of 0.1–0.5 mm and breadth of 9–40mm. Fluorescence induced by lasers and Schlieren imaging were implemented to study the time-dependent liquid flow within the MCHS. Observations indicated that instabilities of the liquid flow present near the lateral walls had a considerable influence on the regime transition in the two-phase flow. Cho and Wang [121] studied flow dynamics, experimentally and numerically, of two-phase flow in MCHS with heterogenous surfaces. The channel surfaces have three hydrophilic channel walls and one hydrophobic one. Both the smooth or rough surfaces were considered for the hydrophobic surface (roughness: 0.226 – 0.550 µm rms (smooth surface) and 21.5 – 28.9 µm (rough surface)). Surface wetting property and roughness were found to affect the liquid flow. Water in liquid form was found to be present preferentially in the two hydrophilic corners with one hydrophobic channel wall. Frequent slug formation occurred in the case of solely hydrophilic channel as compared with channel with a hydrophobic wall. Surface roughness affected two-phase flow. Wang et al. [122] performed analysis of pressure drop fluctuations during two-phase boiling of FC-72 in microchannels with a hydraulic diameter of 0.571 mm, 0.762 mm and 1.454 mm (the aspect ratio (W_{in}/d_{in}) is 20, 20 and 10). Low-amplitude high-frequency fluctuations and high-amplitude low-frequency fluctuations were found to be caused by vapour slug cluster passage and the periodic reversal and rewetting flow respectively. Micro-channel hydraulic diameter was demonstrated to have an impact the pressure drop fluctuation which was found to be significantly chaotic with the increase in channel size.

Keepaiboon and Wongwises [123] examined the flow boiling in a singular rectangular MCHS using R-134a refrigerant as coolant and considering flow patterns and thermal dissipation characteristics. It was determined that flow pattern was affecting the HTC significantly. HTC measured at greater saturation temperatures was found to be higher than values measured at lower saturation temperatures. The HTC was found to rise with the rise in mass flux especially in high heat flux ranges. Thiangtham et al. [124] researched the flow patterns and thermal dissipation characteristics in MCHS (27 channels and a hydraulic diameter of 0.421 mm) during boiling of R-134a. It was determined that variation of flow pattern was sensitive to variation of heat flux and saturation temperature. At lower heat flux, rise in heat flux increased HTC and flow patterns observed were bubbly and slug flow. At higher heat fluxes, HTC rose with rise in mass flux and flow patterns observed were wavy and annular.

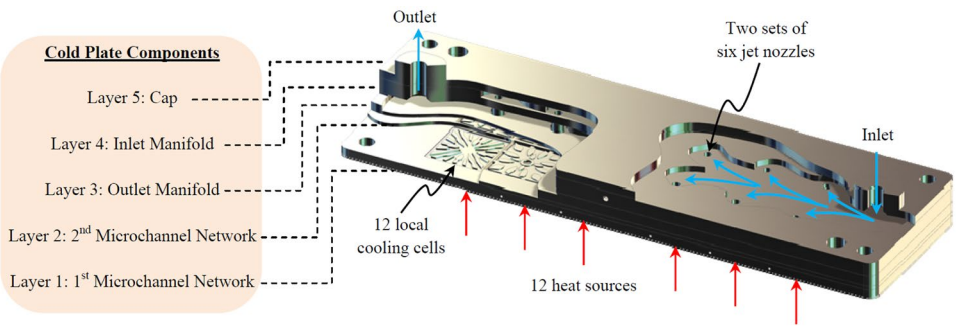

Fig. 33 Multi-pass branching microchannel cold plate [110]

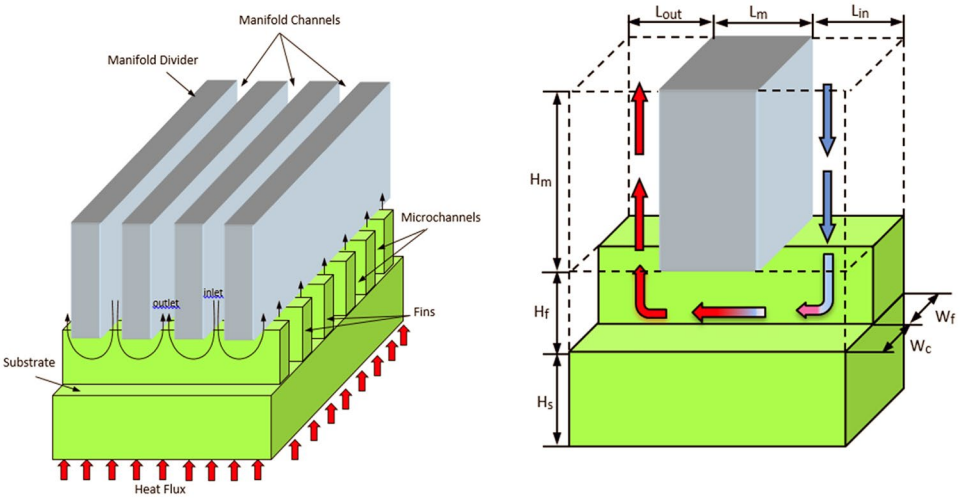

Fig. 34 Schematic of the manifold MCHS [119]

SN	Reference	Enhancement	Solution Method	Dimensions	Working Fluid	Operating parameters	Enhancement Effect
1	Radwan et al. [118]	DL-MCHS	Expt.	W = 0.8 mm H = 0.4 mm	Dehydrated ethanol (C_2H_5OH, 99.5%) Novec-7000, methoxy hepta fluoro propane	concentration ratio (CR) of 5.7 Q = 150W Q_v = 10 - 250 mL/h T_{amb} = 25 °C ± 1 °C	Lower and more uniform solar cell temperatures and improves electrical efficiency at lower flowrates compared with single-phase liquid flow at the same flow rates Parallel flow configuration achieved effective cooling only at higher flowrates in comparison to the counter flow configuration
2	Pourfattah et al. [119]	manifold MCHS	Num.	W = 40 µm H = 200 µm Length of inlet (L_{in}), Length of outlet (L_{out}) = (200, 50), (150, 100), (100, 150), (50, 200) µm Height of manifold, H_m = 500 µm	H_2O/CuO nanofluid (Φ=0.02/0.04)	Re = 25, 50, 75, 100 Constant heat flux, no slip boundary	Increasing the Reynolds number, the effects of in/out ratio become more considerable Increasing the solid concentration of the nanoparticles, the friction coefficient increases due to the enhancement of the effective viscosity
3	Chinnov et al. [120]	Rectangular MCHS	Expt.	W = 9 – 40 mm H = 100 – 500 µm	DI water		
4	Cho and Wang. [121]	Rectangular MCHS	Expt.	1.68 x 1.00 x 150 mm^3	Water	$0.5 \times 10^{-4} \leq U_L \leq 1 \times 10^{-3}$ m/s $0.55 \leq U_G \leq 9.36$ m/s	Surface wetting property and roughness were found to affect the liquid flow. Water in liquid form was found to be present preferentially in the two hydrophilic corners with one hydrophobic channel wall.
5	Wang et al. [122]	MCHS Boiling	Expt.	D_h = 571, 762, 1454 µm Aspect ratio (W_{in}/d_{in}) = 20, 20, 10	Degassed FC-72	q = 0 – 18.31 kW/m^2 G = 11.2, 22.4, 44.8 kg/m^2s	Low-amplitude high-frequency fluctuations and high-amplitude low-frequency fluctuations were found to be caused by vapour slug cluster passage and the periodic reversal and rewetting flow respectively

5 Nanofluids

Nanofluids can be utilized as a replacement of water or water-based coolants. Nanofluids are a stable mixture of base fluid, typically water, and nanoparticles suspended in it forming a colloidal solution which can be considered as single phase and/or multi-phase fluid depending on the volume fraction of the nanoparticles mixed in the base fluid. A surfactant (cetyl trimethyl ammonium bromide (CTAB), polyvinylpyrrolidone, Sodium dodecyl sulphate (SDS), and SDBS etc.) is added to ensure stability of the solution. Nanoparticles generally used are metals (Cu, Zn, Al, Fe etc.) or metal oxides (Al_2O_3, ZnO, CuO etc.). An advantage of nanofluids is the high HTC which can be in the order of over 2 magnitudes greater than the base fluids (Fig. 35) [125]. Several researchers have looked into combining the advantages of nanofluid and MCHS for enhanced heat transfer.

Sarafraz et al. [126] conducted studies characterising fluid flow and thermal dissipation properties of an aqueous-graphene nanoplatelet (GNP) nanofluid in MCHS. Enhancement of the HTC and Nu by approximately 80% was shown using pure water as the baseline. The highest value in pressure drop was by 18.3% and was seen at highest Reynold's number and greatest mass concentration of the GNP nanofluid. Arani et al. [127] studied (numerically) use of nanofluid made with water and single-wall carbon nanotubes (SWCNT) used in a truncated double-layered MCHS as a means of enhancement of heat transfer. The enhancement of Reynolds number, volume fraction of nanoparticles and dimensionless slip velocity coefficient were found to cause substantial increase of heat transfer and decline in thermal resistance of surface. Azizi et al. [128] investigated convective heat transfer in a cylindrical MCHS (Fig. 36) with Cu-H_2O nanofluid as coolant. With 0.05, 0.1 and 0.3 wt% concentration, the Nusselt numbers of nanofluids were increased by approximately 17%, 19% and 23% (Fig. 37) in comparison to values obtained for pure water for similar

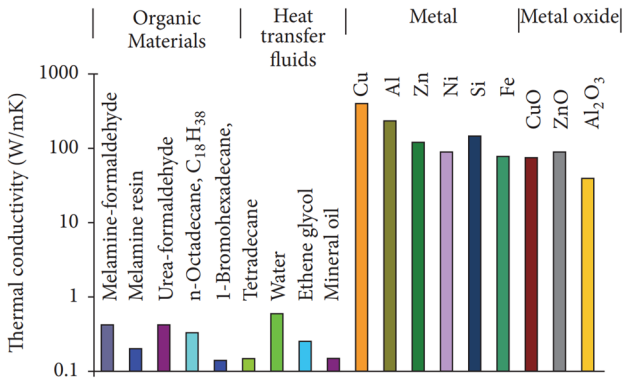

Fig. 35 Thermal conductivity comparison of common polymers, liquids, and solids [125]

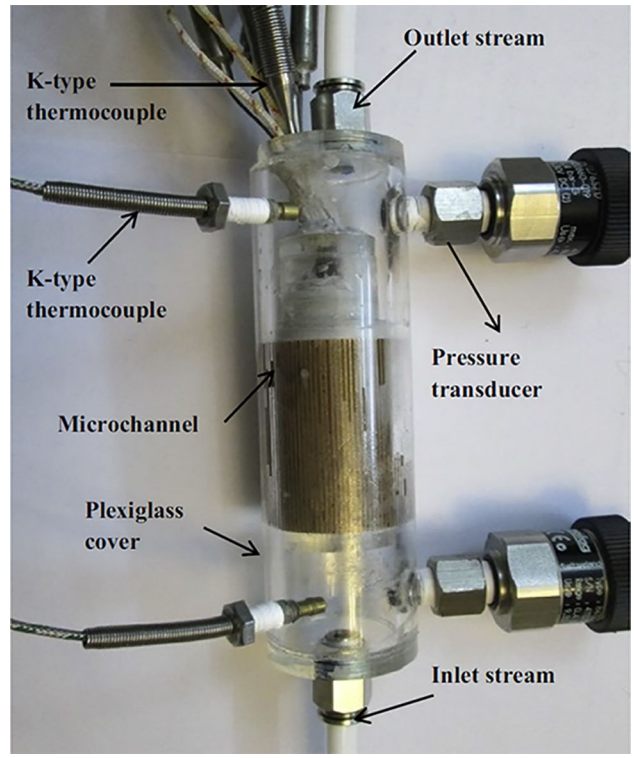

Fig. 36 Cylindrical microchannel heat sink [128]

Reynolds numbers. Reynold's numbers above 900 resulted in a reduction of Nusselt's number.

Bahiraei et al. [129] studied the effectiveness of hybrid (graphene–silver nanoparticles in aqueous solution) nanofluids in MCHS equipped with secondary channels and ribs. A 17% enhancement in the convective HTC was seen with the concentration increasing from 0 to 0.1% at Re = 100.

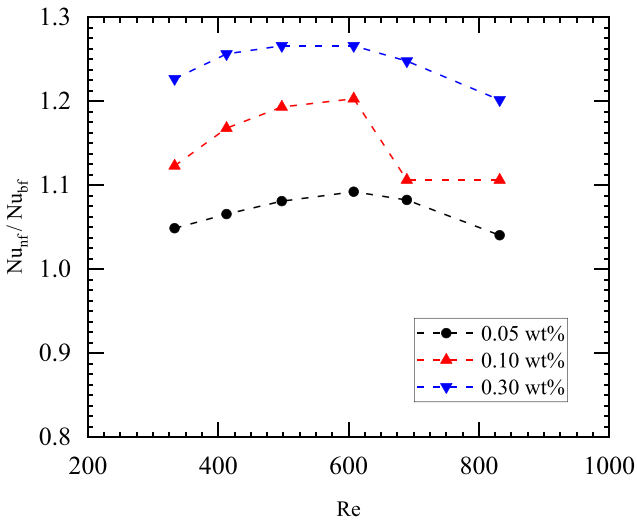

Fig. 37 Nu ratio vs Re for various nanoparticle concentrations using values for pure water as baseline at a constant heat flux of 3.5 W/cm^2 [128]

A reduction of surface temperature by 3.42 K and 13.88 K was seen at Re = 100 to 500. Greater pumping power requirements were experienced at higher Reynold's numbers and concentrations. Hatami et al. [130] researched the use of Cu-H_2O nanofluids in MCHS focusing on thermal and flow analysis. Raising the volume fraction of the nanoparticles, was observed to increase the Brownian motion of the particles (which transmits and disperses thermal energy to the surroundings), thus the coolant and wall temperature differential was found to reduce. Hung et al. [131] investigated the performance with respect to heat transfer with use of (Al_2O_3, SiO_2, CuO H_2O) nanofluid in Double Layered-MCHS. The study indicated a connection between the thermal resistance and channel number. The values of channel width ratio or channel aspect ratio observed were first found to decrease then increase. An average of 26% enhancement in thermal performance was seen with a 1% Al_2O_3- H_2O nanofluid solution over that of pure water. Al-Baghdadi et al. [132] conducted a CFD analysis on (Al_2O_3, SiO_2, CuO H_2O) nanofluid based MCHS. The MCHS working with coolant of Al_2O_3- H_2O was found to have the highest value of the HTC for entire considered range of Reynolds numbers. Tokit et al. [133] conducted studies to determine the thermodynamic performance of an optimized design of interrupted-MCHS (IMCHS) cooled with (Al_2O_3, CuO, and SiO_2 - H_2O) nanofluids. Nu for IMCHS were found to be significantly greater than values observed for conventionally designed MCHS albeit a slightly greater value of drop in pressure. The highest value of thermal augmentation was calculated for alumina based nanofluids, followed by copper oxide based, and then for Silica based nanofluids. Nu was observed to be directly proportionally with the volume fraction of nanoparticle and inversely proportional with the diameter of the nanoparticle.

SN	Reference	Enhancement	Solution Method	Dimensions	Working Fluid	Operating parameters	Enhancement Effect
1	Sarafraz et al. [126]	Graphene Nano-platelet nanofluid	Expt.	Rect CS: 200 × 200 µm Graphene nanoplatelets Thickness = 1.5 – 3 nm length = 123 - 424 nm	GNP nano-fluid	wt% = 0.025 - 0.1 Re = 100-1400	Enhancement of the HTC and Nu by approximately 80% was shown using pure water as the baseline. The highest value in pressure drop was by 18.3%. Nu ratio = (1.05~1.8)
2	Arani et al. [127]	H_2O /single-wall carbon nanotubes (SWCNT) nanofluid with truncated DL- MCHS	Num.	W = 0.05 mm H = 0.45 mm	water/ single-wall carbon nanotubes (SWCNT) nanofluid	q = 106 W/m^2 Re = 500-2000 T_{in} = 300 K P_{out} = 0.1 MPa Vol. Fract = 0, 0.04, 0.08	At λ = 0.4 and 0.8, respectively the minimum and maximum of coefficient of frictions occur Increasing volume fraction of nanoparticles increases the heat transfer rate
3	Azizi et al. [128]	Cu-water nanofluid in a cylindrical MCHS	Expt.	W = 526 µm H = 600 µm Cylindrical CS D_h = 560 µm Particle size = 25 nm	Cu-water nanofluid	wt% = 0.05, 0.1, 0.3 Q_v = 0.5–1.9 L/min Re = 300–800 q = 35 - 50 KW/m^2	Nu enhancement for 0.05, 0.1 and 0.3 wt% concentration 17%, 19% and 23% for plain water and similar Re
4	Bahiraei et al. [129]	MCHS with both secondary channels and ribs	Num.	W = 600 µm, H = 300 µm θ = 45° Length = 500µm 2° gap width = 100 µm Rib Width = 75 µm Rib length = 250 µm	graphene–silver nano-particle water nanofluid	Re = 100 – 500 Φ = 0 - 0.1%	A 17% enhancement in the convective HTC was seen with the concentration increasing from 0 to 0.1% at Re = 100 Greater pumping power requirements were experienced at higher Reynold's numbers and concentrations
5	Hatami et al. [130]	Cu-water nanofluid	Num.	W = 10 – 1000 µm H = 10 – 1000 µm Wall thickness = 10 – 1000 µm Porosity (ε) = 0 – 1 Channel aspect ratio (α_s) = 1–10	Cu - H_2O nanofluid	T_w = 303.04 °C q_w = 1000 W/m^2 Nanoparticle volume fraction (Φ) = 0–0.06	Nusselt number increases with increase in αs due to rise in the interactions between nanoparticles and the solid phase Greater diameter of nanoparticles increases temperature difference between coolant and wall. Nusselt number rises due to improvement in heat transfer mechanism by large nanoparticles with high thermal conductivity.

SN	Reference	Enhancement	Solution Method	Dimensions	Working Fluid	Operating parameters	Enhancement Effect
6	Hung et al. [131]	Double Layered-MCHS with nanofluid	Num.	W = 10 mm H = 0.05 mm particle size 'd' = 38nm Channel number (N) = L_z/ (W_c +W_r) = 35 – 170 width ratio (β) = W_c/ (W_c +W_r) = 0.4 – 0.95 bottom channel aspect ratio (α_1) = H_2/W_c = 2 – 13	Al_2O_3 - H_2O / CuO - H_2O/ TiO_2 - H_2O nano-fluid	Nanoparticle volume fraction (Φ) = 0.5–5% q_w = 70 W/cm^2	The values of channel width ratio or channel aspect ratio observed were first found to decrease then increase An average of 26% enhancement in thermal performance was seen with a 1% Al_2O_3 - H_2O nanofluid solution over that of pure water.
7	Al-Baghdadi et al. [132]	Nanofluid in rec MCHS	Num.	W = 0.1 mm H = 0.2 mm	SiO_2 - H_2O / Al_2O_3 - H_2O / CuO - H_2O nanofluid	Re = 100 - 1000 q = 1 MW/m^2 Volume fraction (Φ) = 1 - 10 %	The MCHS working with coolant of Al2O3- H2O was found to have the highest value of the HTC for entire considered range of Reynolds numbers
8	Tokit et al. [133]	Nanofluid in interrupted MCHS	Num.	W = 0.057 mm 0.01 at minima (interrupted MCHS) H = 0.18 mm	SiO_2 - H_2O / Al_2O_3 - H_2O / CuO - H_2O nanofluid	q = 650 kW/ cm^2 Re = 140 - 1089	Nu for IMCHS were found to be significantly greater than values observed for conventionally deigned MCHS albeit a slightly greater value of drop in pressure.
9	Vinoth et al. [134]	Nanofluid in oblique finned triangular/ pentagonal CS MCHS	Expt.	W = 800 µm H = 900 µm θ = 26°	CuO - H_2O (0.3%), Al_2O_3 - H_2O (0.3%), Al_2O_3 -CuO - H_2O (0.3%) Hybrid nanofluid	q = 50 kW/m^2 Q_v = 0.1 - 0.5 L/min	Enhancement of the rate of thermal dissipation and reduction in pressure drop by more than 12.34% and 16.5% respectively was observed as compared to the triangle shaped cross section MCHS The pentagonal MCHS resulted in results with superior thermal dissipation and flow characteristics

6 Applications

In the previous sections, different geometry, working fluids, and solution approaches are discussed thoroughly. Each of these mentioned studies were obviously investigated for a certain application of microchannels in the various engineering fields. Microchannels have been developed for high heat flux removal applications with compact geometric requirements. These unique set of challenges exist in a wide area of applications. In the subsequent section, few of those applications are discussed.

6.1 Cooling of electronic circuits

The power densities seen in commercial and consumer grade electronics have been on the rise [2, 135] and effective cooling along with compactness of design are increasingly being sought after [1, 3]. Several cooling techniques are being investigated, microjet cooling [136], PCM [137], microchannel cooling etc. In this section we will look at the use of microchannel either as a standalone system or as a part of a combination of technologies being developed or used in electronic circuits.

Jiang et al. [138] experimented with the use of Electroosmotic Microchannel closed-loop cooling system for thermal management in VLSI circuits (Fig. 38). Results indicated the ability of the system to remove 38 W/cm^2 and maintain the temperature of the chip below 100 °C.

Chen et al. [139] investigated the use of interconnected microchannels with re-entrant cavities (IMRCs) for pool boiling enhancement deionized water as the working fluid for cooling of high-powered electronics. IMRCs exhibit a significant rise in pool boiling heat transfer as compared with results obtained for smooth copper plates (SCPs). Silvério et al. [140] developed and tested an integrated multi-microchannel heat sink (27 rectangular channels in parallel with

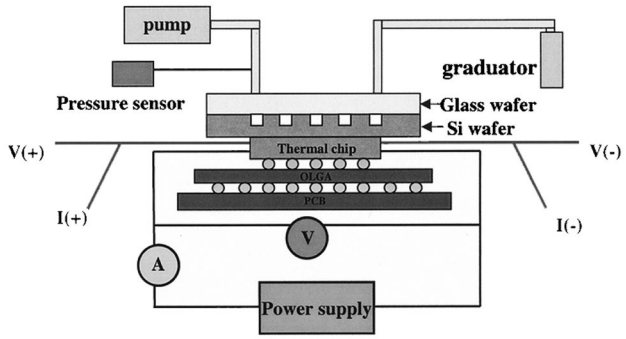

Fig. 38 Experimental apparatus for characterization of the MCHS heat exchanger [138]

hydraulic diameter D_h= 0.096 mm, L/D_h= 104 and relative roughness of 2.4%) for electronics cooling. Results indicated, in the absence of latent cooling, the chip temperature was maintained below 358 K ($T_{w,\,avg}$= 338.4 K). The heat flux measured at the peak was 108 kW/m^2 and a corresponding flow rate of 3.050 L/h. With latent heat cooling, the heat flux extracted rose to 266 W•m^2 for a corresponding flow rate of 1.300 L/h (Re = 277). Bahiraei et al. [141] studied MCHS (Fig. 39) with hybrid nanofluid with regards to thermodynamic performance and 2nd law characteristics. The nanofluid used contained graphene–silver nanoparticles. Surface temperature was determined to reduce by increasing either velocity or concentration. The maximum temperature observed on the heating surface was found to reduce by raising the concentration and velocity at the inlet, reducing the chances of formation of hot spots.

Hou et al. [142] investigated the use of two-phase flow (with refrigerant R1234yf) microchannel thermal management systems (Fig. 40) for power electronics with heat dissipation of over 500 W/m^2 with a maximum heat flux of about 750 W/m^2. From observations, the thermal management system had the capacity to handle a heat flux of 5260 kW/m^2 while maintaining the junction under 120 °C.

Jaikumar and Kandlikar [143] studied using open MCHS with porous fin on tops and with FC-87 as the coolant used for enhanced pool boiling for cooling of electronics. A peak value of CHF of 370 kW/m^2 was attained (270 % improvement using plain chip as baseline). The improvement in pool boiling was attained due to presence of additional nucleation sites and/or rise in the area available for thermal dissipation. Jung et al. [144] researched methods for cooling of power electronics with high fluxes in excess of 10 MW/m^2. For single- and two-phase, Water and R245fa refrigerant were used as working fluids respectively. The three cooling methods investigated were the device substrate copper cold-plate with bonded MCHS module, the device substrate with embedded MCHS directly etched into it and 3D manifold with inlet and outlet module on embedded MCHS. The first method provided the least thermal resistance. Laguna et al. [145] investigated the use of microfluidic cell cooling for electronics. From observations, temperature uniformity was enhanced along the whole system while lowering requirements of pumping power by 89.2 % in comparison to the baseline as measured for conventional MCHS technology.

Sakanova et al. [146] performed optimization and comparative studies of DL-MCHS and double sided MCHS with water/Alumina nanofluid for cooling of power electronics. The microchannels were incorporated within the Copper-layer of direct bond copper. Based on the optimal geometry, the sandwich structure with counter flow in comparison to single layer (SL), DL with unidirectional flow and DL with counter flow, showed a decline in thermal resistance by 59%, 52% and 53% respectively. Sharma et al. [147] conducted energy efficient hotspot targeted optimized MCHS etched onto the reverse side of the chips for thermal management of the electronics. For a value of 1500 kW/m^2 and 3000 kW/m^2 as heat flux at the hotspot, the requirement of the pumping power for optimized designs was determined to be 0.23% and 0.17% respectively of the total power consumption by the chip.

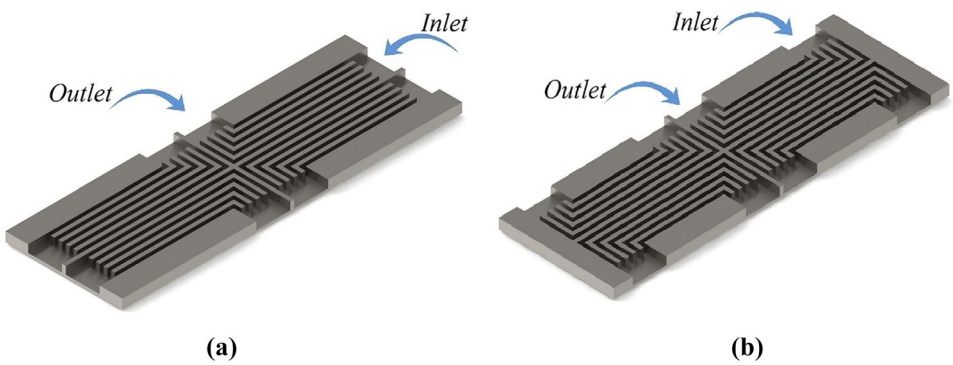

Fig. 39 The MCHS being studied: (**a**) heat sink type A, (**b**) heat sink type B. [141]

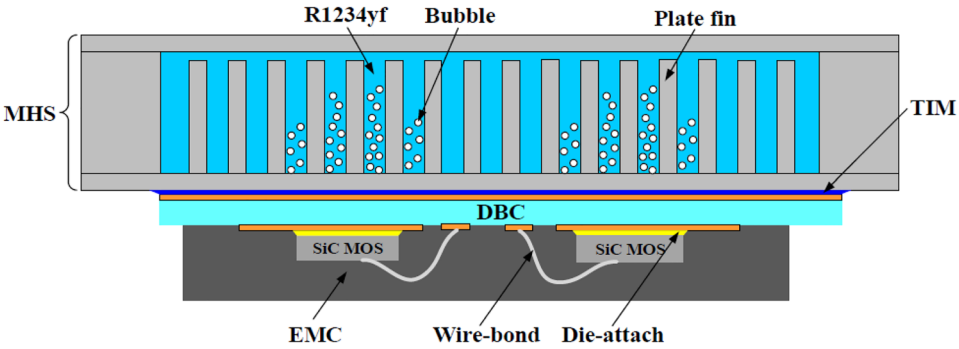

Fig. 40 SiC power module assembly on the MCHS with two-phase flow boiling [142]

6.2 As heat exchangers

Redo et al. [148] performed characterization studies of two-phase flow of R410a. The flow was simulated for air-conditioning systems within the vertical header of a microchannel heat exchanger (MCHE) with multiple horizontally oriented microchannel flat tubes. Pan et al. [149] examined the performance of MCHE with fan shaped cavities (FSC) with regards to heat transfer. Effects of structural parameters on the performance of the MCHE was studied. The performance of the MCHE with FSCs, from the results, indicate that it is superior to that without FSCs and has a lower pressure drop. Hu et al. [150] established experimentally the impact of outdoor air-side fouling on frost growth on thermal dissipation characteristics of a MCHE for a heat pump outdoor coil. Fouling induced reduction in initial airflow by about 3.5% was found to increase thermal dissipation and growth rates of frost. Heavier fouling was found to decrease both rates. When growth of frost was normalized to thermal dissipation, it was determined to be enhanced by fouling. Mahvi and Garimella [151] studied two-phase flow distribution of saturated R134a refrigerant in MCHE headers with several header geometries (Fig. 41). It was observed that the liquid distribution remained nearly constant as the inlet quality was raised, but there was a marked improvement in vapor distribution.

At low qualities there exist restrictions on the drop in pressure across each flow path. This forces the liquid to distribute more uniformly and enhance the overall distribution. It was determined that the distribution was not greatly affected by the header inlet mass flux. It was observed that greater quantities of liquid were transported to downstream channels by the rise in the momentum of the liquid phase in the header. This, however, resulted in low liquid flow rates in the channels closest to the inlet port. Glazar et al. [152] investigated the effects of different microchannel shapes in compact heat exchangers using an open wind tunnel. Results showed that effectiveness of heat transfer reduced with the increase of air velocity at inlet. The optimal results were attained with microchannels of hexagonal and diamond shape. However, lowest pressure drop was observed in rectangular shapes cross section. Kwon et al. [153] investigated the application of air-cooled MCHE (cross flow, 1 cm^3, R245fa refrigerant) for high power density applications. A maximum power density of 60 MW/m^3 was measured for an air inlet temperature of 27 °C refrigerant inlet temperature at 80 °C.

Li and Hrnjak [154] performed validation studies for lubrication effect incorporated model of MCHE. A new model was developed and validated against experimental results (R134a-PAG 46 oil) at different circulation ratios for oil (0.1%-8.3%). Results from numerical studies showed that addition of lubricant improved distribution

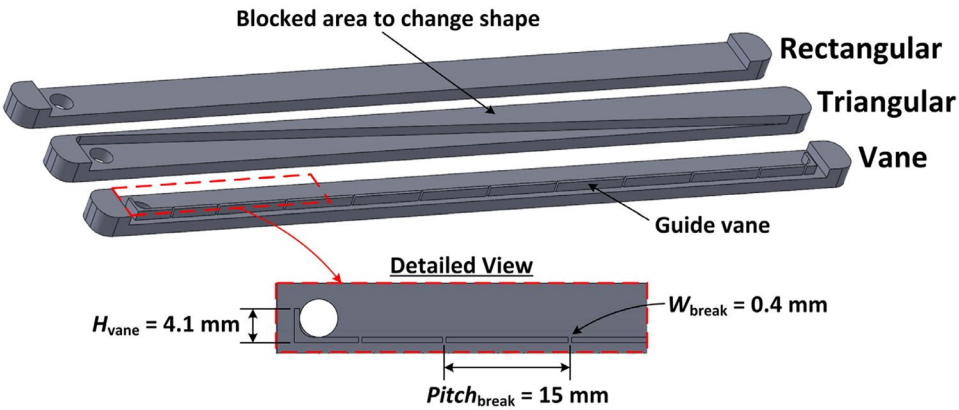

Fig. 41 Header geometries investigated [151]

of refrigerant. Mazaheri et al. [155] developed a four layer MCHE (counter-current arrangement) (Fig. 42) and conducted two-phase flow analysis with nanofluid flow. The nanofluid was taken as the Hot fluid, while for the cold fluid, water was selected. Nanoparticles improved the heat exchange capacity and led to better performing heat exchange rate. Increase in channel number resulted greater overall HTC owing to greater and intense impingement of flow which causes greater disruption of the thermal boundary layer.

Mohammadian et al. [156] conducted studies on two-phase flow counter flow MCHE (CFMCHE) with alumina/water nanofluid flow. Reducing particle size and raising concentration of nanoparticles was found to have superior effectiveness, lower pumping power as well as a reduction of temperature within the solid phase of CFMCHE. Reynolds number was found significantly affect the performance of system with its' reduction was found to increase the effectiveness while the thermal dissipation contribution of entropy was also seen to reduce. The pumping and frictional power contribution of entropy was found to reduce with decrease of Reynold's Number. Shi et al. [157] used surrogate model coupled with genetic algorithm to optimize the inlet of ceramic MCHE. By optimization, the fluid flow nonuniformity was lowered by 68.2% and decrease in the drop in pressure was by 6.6%. This resulted in the fluid flow uniformity in the heat exchanger improving substantially albeit with the penalty of a small pressure drop. Yih and Wang [158] characterised the thermo-hydraulic performance of a MCHE for the purpose of waste heat recovery. The overall heat transfer increased with air flow while the effectiveness decreased with air flow for a given oil flow rate. With an increase in air inlet temperature, the effectiveness was found to increase. A higher thermal conductivity was attributed to this. Zhou et al. [159] examined the flow and heat transfer properties of parallel-flow double layered MCHE (Fig. 43). The increasing height and width were found to influence the velocity profile. Greater widths and lower heights were determined to increase average Nusselt number for simultaneously thermally and hydrodynamically developing flow.

Zhou et al. [160] investigated the flow and heat transfer properties of MCHE embedded with different shape micropillars (Fig. 44). From the results, the Nu/Nu_0 ratio for micropillars of type A, B and C was found to be 1.65–1.9, and for micropillars of type D and E, was 1.6–1.7. A 20–40% increase in the pressure loss was however observed in the type D and E as compared to microchannel without micropillars, and an increase of above 60% for the type A, B and C.

6.3 As heat pipes

Heat pipes are heat-transfer devices which combine the concepts of both thermal conductivity and phase transition to effectively move heat between two solid interfaces. Due to the very HTC for boiling as well as for condensation applications, heat pipes are considered to be very effective thermal conductors.

Wei et al. [161] studied the mechanisms of flow and heat transfer using CFD analysis under zero gravity conditions of a Ω-shape microchannel aluminium-ammonia grooved heat pipe (GHP) (Fig. 45). Results indicated that the GHP was adept of moving thermal energy over relatively large distances with a small difference of temperature. Li et al. [162] examined the thermodynamic performance of microchannel heat pipe (MCHP) at varied tilt angles and evaporator temperatures. The heat pipe consisted of 2 flat-panel MCHS in parallel. Each microchannel was equipped with micro-fins

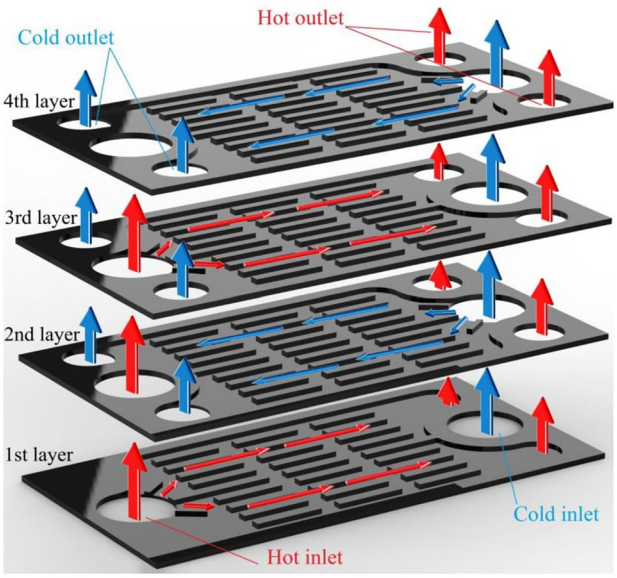

Fig. 42 Arrangement of the 4-layer MCHE w/implemented arrangement of flow [155]

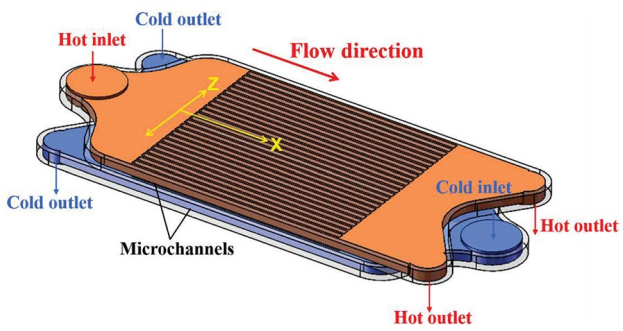

Fig. 43 Parallel - flow double layered MCHE [159]

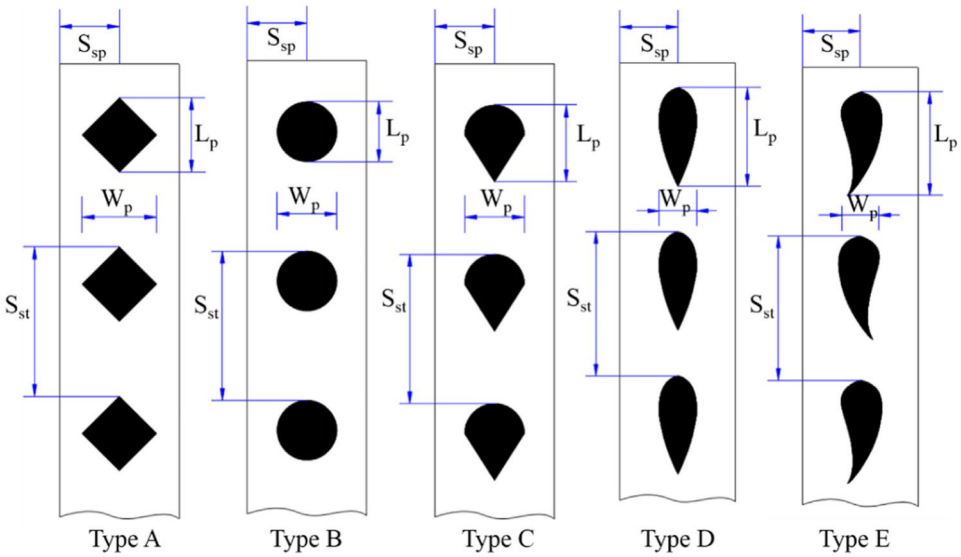

Fig. 44 Top view of micropillars with different shapes [160]

to augment transfer of heat. The working fluid undergoes phase change in the evaporator side and is transported to the condenser side due to pressure differential created due to temperature difference. The latent heat is released at the condenser side, and the working fluid condenses undergoing phase change (back to liquid form) and drawn back to the evaporator side usually by means wicking effect. The fluctuations in temperature observed in the MCHP were found to increase proportionally with the tilt angle. This fluctuation was attributed to the effect of gravity. The temperature difference was found to increase with the increase of evaporator temperature at low tilt angle. However, relation between the variation of the temperature difference and evaporator temperatures whilst at higher tilt angle was no longer a simple one.

Modjinou et al. [163] performed research comparing different temperature management systems for photovoltaic devices. They compared macro encapsulated phase change materials (PCM), MCHP and conventional thermal management systems using mathematical models, experimentation, and simulation. The results indicated 36.71%, 35.53% and 31.78% respectively to be the combined average photo-thermal and electrical efficiency. As compared to the other solutions, MCHP had the advantage of passively and effectively transferring and absorbing heat. R134a was used as refrigerant and copper was simulated instead of aluminium for the MCHP to prevent faster freezing damages. Aluminium is known to diffuse heat better while copper, as a heat transfer media, is known to be a better. Thus, to achieve steady state faster, MCHP using copper as material is preferred over those made with aluminium. Li et al. [164, 165] developed and performed analysis of a MCHP present in an evacuated tube solar collector with an integrated thermoelectric generation system, the structure of which is shown in Fig. 46. The solar radiation impinges on the MCHP evaporator and is absorbed due to the selective absorbing coating. The heat is conducted through Thermoelectric generator (TEG) is rejected to the cooling water, thereby increasing the electrical output generated by TEG. The results indicated a superior thermal performance of the system with the advantage of electricity production.

Shittu et al. [166] conducted a study experimentally as well as analysis of exergy of photovoltaic-thermoelectric with flat plate microchannel. The hybrid photovoltaic-thermoelectric was able to exploit a broader solar spectrum thus converting

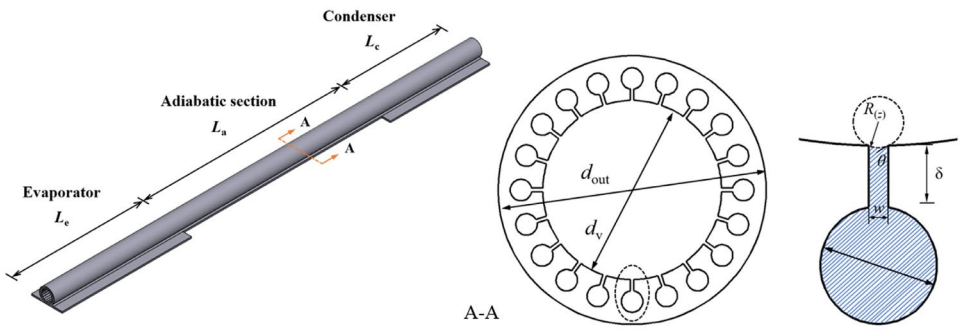

Fig. 45 Ω-shape grooved heat pipe [161]

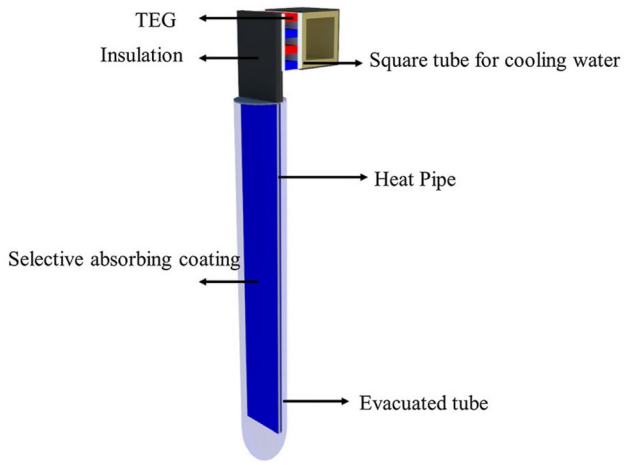

Fig. 46 MCHP equipped evacuated tube solar collector with an integrated thermoelectric generation system [164]

more energy from the sun while enhancing electrical conversion efficiency of PV system by effective cooling. Results showed a marked improvement over PV only systems and uncooled PV systems. In addition, heat water was made available for domestic or industrial consumption. 69.53% and 56.57% were the highest and lowest thermal efficiencies obtained respectively.

Song et al. [167] developed a hybrid condenser equipped heat pump. The hybrid condenser combined a flat plate MCHP with a thermoelectric generator (TEG) and Fresnel photovoltaic (FPV) evaporator. The TEG was fitted between the CPV and absorber plate in the evaporator. It can be used to convert the thermal energy contained in the PV into electricity. This, however, inhibited the dissipation of heat from the PV, thus adversely impacting the performance of the PV. The TEG was found to improve the electrical and total performance of the system if TEG is placed in the condenser. This was done to convert the thermal energy that would be rejected into electrical energy without impacting the heat dissipation capacity of PV. The MCHP collects thermal energy from condenser to attain a large density of heat flow as well as a high output of TEG. The setup with the TEG in this configuration, shows an improvement of electrical efficiency by 10.83% and improvement of total exergy efficiency by 6.02%.

6.4 Thermal management of photovoltaic cells

Solar power is a key area where cooling technologies are being researched and new technologies developed. There exists a correlation between photovoltaic efficiency with the temperature of the photovoltaic (PV) cells. In addition, with the use of concentrated photovoltaics (CPV) which experience high solar concentration ratios and attain elevated temperatures, (and have conversion efficiencies up to 46% as compared to 20% for flat plate collectors), the temperature of the cells turns into a critical parameter [168]. Thus, there is a need to provide effective cooling for these systems to reach peak net output power whilst ensuring the safe operation of the system components.

Abo-Zahhad et al. [169] investigated stepwise variation of width microchannel cooling in thermal management application in high concentrator solar cells. Various parameters such as the cell temperature, electrical efficiency, thermal efficiency, electrical thermal, and total exergy efficiency, and thermal resistance of the heat sinks were shown, from the results, to be impacted by the design of the heat sink as well as the mass flow rate of the coolant. At a concentration ratio of 1000 suns and elevated coolant flowrate (1000 from 25 g/min), saw a drop in the temperature of the solar cell (344.7 K to 313 K) with non-uniformity of the temperature in the solar cell reducing from 288.5 K to 282 K. Acharya [170] studied the flow and thermal characteristics of a hybrid Alumina–copper/ water nanofluid flow within a MCHS impinged by radiative solar energy. From observation, solar radiation fostered transport of heat at suction. A lower velocity profile was observed for suction with the use of hybrid nanofluid in comparison to ordinary nanofluid. However, a completely opposite phenomenon was observed whilst injection. Ahlatli et al. [171] examined the thermal performance of carbon nanotube nanofluids (0.01%, 0.05%, 0.1%, and 0.5% weight fraction) in solar collectors with microchannels . The measured heat transfer, pressure drop, and pump power increased with the rise of the weight fraction of nanofluids. With the use of nanofluids, the heat transfer was found to be greater than that of the (distilled water) base fluid. With quartz being used at the upper surface of the MCHE resulted in the high-weight-fraction nanofluids becoming more effective.

7 Conclusions and future scope

This review included different geometric designs, coolant phases, types, and application of microchannels currently being investigated which has tremendous applications in the different engineering domains. The review is primarily focused on the various geometric designs of the microchannels, coolants used as well as the operating modes which are derived and optimized with the help of numerical simultion and extensive experimentation. It is vital to appreciate the factors such as thermal conductivity, thermal resistance, and fluid flow distribution in the microchannels which influence the thermodynamic performance and drop in pressure as observed in the microchannels.

The review looked at the different commonly used structures of MCHS. Different coolant combinations and performance of each was also discussed. Six structures were

looked at: straight microchannels, wavy microchannels, pin-fin microchannels, oblique finned microchannels, porous microchannels and microchannels with nanostructures. It was determined that while each of these microchannels had their unique advantages, though the simpler geometry of straight microchannels provided an economical shape for ease of manufacturing, the microchannels with relatively complex shapes provided a greater HTC in comparison with the straight microchannels. The advantages arose from the ability of the microchannels to cause redevelopment of the thermal boundary layer, thus reducing the resistance to heat transfer to the coolant. As a result, a significant increase in Nusselt number was observed. Use of variation in location, geometry, and number of microchannels also had the advantage of being able to be used for hotspot mitigation. The geometries however also increased the resistance to flow thus increasing the pumping power requirements. Use of different working fluids was also looked at. Use of single-phase system simplified the implementation by eliminating the complexity of modelling phase transitions. This however, also limited the amount of heat transfer to the coolant as it was limited by sensible heat capacity of the fluids. In Two-phase systems, the latent heat capacity of the fluid is also utilized. This greatly improves the usable heat capacity of the fluid. Tools have been developed to predict flow and heat transfer as well as to predict the onset of dry out. Use of nanofluids in MCHS was also looked at. Nanofluids offer HTC ranges which are magnitudes higher than those observed in single-phase and in some two-phase systems. There was a marked increase of Nusselt number observed for comparable Reynold's numbers in case of nanofluid flow vs single-phase fluid flow. Several combinations of nanofluid were investigated. Studies have been conducted using experimental setups as well as numerically. The numerical studies offered the option of use of complex physical structures as well as conditions (constant heat flux, absence of gravity etc.) which would have been difficult to recreate. Numerical techniques were also used for different optimization studies. Purely experimental studies as well as some analytical studies were also looked at. Some of the applications of MCHS for thermal management in electronic circuits, heat exchangers, heat pipes in photovoltaic cells were also looked at. Uses in VLSI, hotspot mitigation in electronics, waste heat recovery systems, combined solar and heating systems were covered. In each, the use of microchannels and related technology helped improve the performance of the system.

From the above it is clear that significant work has been carried over the years by numerous researchers broadening our knowledge in the domain and pushing the boundaries of science. Combining design features is one promising method to improve achievable performance. Further studies could include the use of hydrophilic and hydrophobic coatings as well as other nanostructures in MCHE and MCHP to aid in heat transfer as the study is limited. Use of such treatments could enhance the removal of heat and improve the performance of MCHE & MCHP. Similarly, research into geometries that allow the rapid removal of nucleating bubbles and slugs away from the heat transfer surface can be furthered and combined for improving heat transfer along with the further development of designs that are more rapidly deployable. Use of bio inspired surfaces for the purpose of heat transfer enhancement and drag reduction can also be further researched and incorporated into designs.

Funding This research did not receive any specific grant from funding agencies in the public, commercial, or not-for-profit sectors.

Data availability Data will be available on request.

Declarations

Conflict of interest The authors declare that there is no conflict of interest.

References

1. Fan Y, Winkel C, Kulkarni D, Tian W (2018) Analytical Design Methodology for Liquid Based Cooling Solution for High TDP CPUs. Proc 17th Intersoc Conf Therm Thermomechanical Phenom Electron Syst ITherm 582–6
2. Huang S, Xiao S, Feng W (2009) On the energy efficiency of graphics processing units for scientific computing. IPDPS 2009 - Proc 2009 IEEE Int Parallel Distrib Process Symp
3. Van Wyk JD, Lee FC (2013) On a future for power electronics. IEEE J Emerg Sel Top Power Electron. 1(2):59–72
4. Gilmore N, Timchenko V, Menictas C (2017) Microchannel cooling of concentrator photovoltaics: A review. Renew Sustain Energy Rev 2018(90):1041–59
5. Naqiuddin NH, Saw LH, Yew MC, Yusof F, Ng TC, Yew MK (2017) Overview of micro-channel design for high heat flux application. Renew Sustain Energy Rev 2018(82):901–14
6. Başaran A, Yurddaş A (2021) Thermal modeling and designing of microchannel condenser for refrigeration applications operating with isobutane (R600a). Appl Therm Eng 198
7. Ohadi M, Choo K, Dessiatoun S, Cetegen E (2013) Next Generation Microchannel Heat Exchangers. Springer Briefs Appl Sci Technol 1–111
8. Palm B (2001) Heat transfer in microchannels. Microscale Thermophys Eng 5(3):155–75
9. Deng D, Zeng L, Sun W (2021) A review on flow boiling enhancement and fabrication of enhanced microchannels of microchannel heat sinks. Int J Heat Mass Transf 175:121332
10. Devahdhanush VS, Lei Y, Chen Z, Mudawar I (2021) Assessing advantages and disadvantages of macro- and micro-channel flow boiling for high-heat-flux thermal management using computational and theoretical/empirical methods. Int J Heat Mass Transf 169:120787
11. Cheng P, Wang G, Quan X (2009) Recent work on boiling and condensation in microchannels. J Heat Transfer 131(4):1–15
12. Kumar K, Kumar P (2021) Effect of groove depth on hydrothermal characteristics of the rectangular microchannel heat sink. Int J Therm Sci 161(October 2019):106730
13. Law M, Lee PS (2015) A comparative study of experimental flow boiling heat transfer and pressure characteristics in

straight- and oblique-finned microchannels. Int J Heat Mass Transf 85:797–810
14. Alam T, Lee PS, Yap CR, Jin L (2013) A comparative study of flow boiling heat transfer and pressure drop characteristics in microgap and microchannel heat sink and an evaluation of microgap heat sink for hotspot mitigation. Int J Heat Mass Transf 58(1–2):335–47
15. Mathew J, Lee PS, Wu T, Yap CR (2020) Comparative Study of the Flow Boiling Performance of the Hybrid Microchannel-Microgap Heat Sink with Conventional Straight Microchannel and Microgap Heat Sinks. Int J Heat Mass Transf 156:119812
16. Balasubramanian K, Lee PS, Jin LW, Chou SK, Teo CJ, Gao S (2011) Experimental investigations of flow boiling heat transfer and pressure drop in straight and expanding microchannels - A comparative study. Int J Therm Sci 50(12):2413–21
17. Balasubramanian K, Jagirdar M, Lee PS, Teo CJ, Chou SK (2013) Experimental investigation of flow boiling heat transfer and instabilities in straight microchannels. Int J Heat Mass Transf 66:655–71
18. Jasperson BA, Jeon Y, Turner KT, Pfefferkorn FE, Qu W (2010) Comparison of micro-pin-fin and microchannel heat sinks considering thermal-hydraulic performance and manufacturability. IEEE Trans Components Packag Technol 33(1):148–60
19. Xia G, Ma D, Zhai Y, Li Y, Liu R, Du M (2015) Experimental and numerical study of fluid flow and heat transfer characteristics in microchannel heat sink with complex structure. Energy Convers Manag 105:848–57
20. Miner MJ, Phelan PE, Odom BA, Ortiz CA (2013) Experimental measurements of critical heat flux in expanding microchannel arrays. J Heat Transf 135(10)
21. Lee HJ, Liu DY, Yao SC (2010) Flow instability of evaporative micro-channels. Int J Heat Mass Transf 53(9–10):1740–9
22. Xie G, Shen H, Wang CC (2015) Parametric study on thermal performance of microchannel heat sinks with internal vertical Y-shaped bifurcations. Int J Heat Mass Transf 90:948–58
23. Mondal B, Pati S, Patowari PK (2021) Serpentine square wave microchannel fabrication with WEDM and soft lithography. Mater Today Proc 46(xxxx):8513–8518
24. Khoshvaght-Aliabadi M, Hosseinirad E, Farsi M, Hormozi F (2021) Heat transfer and flow characteristics of novel patterns of chevron minichannel heat sink: An insight into thermal management of microelectronic devices. Int Commun Heat Mass Transf 122(February):105044
25. Peng Y, Li Z, Li S, Cao B, Wu X, Zhao X (2021) The experimental study of the heat ransfer performance of a zigzag-serpentine microchannel heat sink. Int J Therm Sci 163(January):106831
26. Xia GD, Jiang J, Wang J, Zhai YL, Ma DD (2015) Effects of different geometric structures on fluid flow and heat transfer performance in microchannel heat sinks. Int J Heat Mass Transf 80:439–47
27. Zhou J, Hatami M, Song D, Jing D (2016) Design of microchannel heat sink with wavy channel and its time-efficient optimization with combined RSM and FVM methods. Int J Heat Mass Transf 103:715–24
28. Ahmed MA, Shuaib NH, Yusoff MZ (2012) Numerical investigations on the heat transfer enhancement in a wavy channel using nanofluid. Int J Heat Mass Transf 55(21–22):5891–8
29. Feng Z, Hu Z, Lan Y, Huang Z, Zhang J (2021) Effects of geometric parameters of circular pin-fins on fluid flow and heat transfer in an interrupted microchannel heat sink. Int J Therm Sci 165(February):106956
30. Ferster KK, Kirsch KL, Thole KA (2018) Effects of geometry, spacing, and number of pin fins in additively manufactured microchannel pin fin arrays. J Turbomach 140(1):1–10
31. Lan Y, Feng Z, Huang K, Zhang J, Hu Z (2021) Effects of truncated and offset pin-fins on hydrothermal performance and entropy generation in a rectangular microchannel heat sink with variable fluid properties. Int Commun Heat Mass Transf 124(April):105258
32. Soleymani Z, Rahimi M, Gorzin M, Pahamli Y (2020) Performance analysis of hotspot using geometrical and operational parameters of a microchannel pin-fin hybrid heat sink. Int J Heat Mass Transf 159:120141
33. Tullius JF, Tullius TK, Bayazitoglu Y (2012) Optimization of short micro pin fins in minichannels. Int J Heat Mass Transf 55(15–16):3921–32
34. Alam MW, Bhattacharyya S, Souayeh B, Dey K, Hammami F, Rahimi-Gorji M et al (2020) CPU heat sink cooling by triangular shape micro-pin-fin: Numerical study. Int Commun Heat Mass Transf 112:104455
35. Bhandari P, Prajapati YK (2021) Thermal performance of open microchannel heat sink with variable pin fin height. Int J Therm Sci 159(August 2019):106609
36. Jia Y, Xia G, Li Y, Ma D, Cai B (2018) Heat transfer and fluid flow characteristics of combined microchannel with cone-shaped micro pin fins. Int Commun Heat Mass Transf 92:78–89
37. Mei D, Lou X, Qian M, Yao Z, Liang L, Chen Z (2014) Effect of tip clearance on the heat transfer and pressure drop performance in the micro-reactor with micro-pin-fin arrays at low Reynolds number. Int J Heat Mass Transf 70:709–18
38. Saravanan V, Umesh CK (2018) Numerical comparison for thermo-hydraulic performance of pin fin heat sink with micro channel pin fin heat sink. Sadhana - Acad Proc Eng Sci 43(7):1–15
39. Lee YJ, Lee PS, Chou SK (2010) Enhanced microchannel heat sinks using oblique fins. Proc ASME InterPack Conf 2009 2:253–60
40. Lee YJ, Lee PS, Chou SK (2010) Experimental investigation of silicon-based oblique finned microchannel heat sinks. 2010 14th Int Heat Transf Conf IHTC 14 6:283–291
41. Lee YJ, Lee PS, Chou SK (2010) Experimental investigation of oblique finned microchannel heat sink+. In: 2010 12th IEEE Intersoc Conf Thermal Thermomechanic Phenomena Electron Sys 1–7
42. Lee YJ, Lee PS, Chou SK (2012) Enhanced thermal transport in microchannel using oblique fins. J Heat Transfer 134(10):1–10
43. Ansari D, Husain A, Kim KY (2010) Optimization and comparative study on oblique-and rectangular-fin microchannel heat sinks. J Thermophys Heat Transf 24(4):849–52
44. Law M, Lee PS (2015) Comparative Study of Temperature and Pressure Instabilities during Flow Boiling in Straight-and 10°Oblique-Finned Microchannels. Energy Procedia 75:3105–12
45. Law M, Kanargi OB, Lee PS (2016) Effects of varying oblique angles on flow boiling heat transfer and pressure characteristics in oblique-finned microchannels. Int J Heat Mass Transf 100:646–60
46. Lee YJ, Lee PS, Chou SK (2013) Hotspot mitigating with obliquely finned microchannel heat sink-an experimental study. IEEE Trans Components, Packag Manuf Technol 3(8):1332–41
47. Lee YJ, Singh PK, Lee PS (2015) Fluid flow and heat transfer investigations on enhanced microchannel heat sink using oblique fins with parametric study. Int J Heat Mass Transf 81:325–36
48. Mou N, Lee YJ, Lee PS, Singh PK, Khan SA (2016) Investigations on the influence of flow migration on flow and heat transfer in oblique fin microchannel array. J Heat Transf 138(10):1–13
49. Vinoth R, Kumar DS (2017) Channel cross section e ff ect on heat transfer performance of oblique fi nned microchannel heat sink. Int Commun Heat Mass Transf 87(August):270–6
50. Vinoth R, Kumar DS (2018) Experimental investigation on heat transfer characteristics of an oblique finned microchannel heat sink with different channel cross sections. Heat Mass Transf und Stoffuebertragung 54(12):3809–17

51. Vinoth R, Senthil Kumar D (2018) Numerical study of inlet cross-section effect on oblique finned microchannel heat sink. Therm Sci 22(6):2747–57
52. Lan X, Xie G, Ji S, Tang Q, Li X, Wang X et al (2021) Experimental and numerical study on the temperature uniformity of a variable density alternating obliquely truncated microchannel. Int J Heat Mass Transf 176:121440
53. Panse SS, Ekkad SV (2021) A numerical parametric study to enhance thermal hydraulic performance of a novel alternating offset oblique microchannel. Numer Heat Transf Part A Appl 79(7):489–512
54. Far BR, Mohammadian SK, Khanna SK, Zhang Y (2015) International Journal of Heat and Mass Transfer Effects of pin tip-clearance on the performance of an enhanced microchannel heat sink with oblique fins and phase change material slurry. HEAT MASS Transf 83:136–45
55. Jiang PX, Fan MH, Si GS, Ren ZP (2001) Thermal-hydraulic performance of small scale micro-channel and porous-media heat-exchangers. Int J Heat Mass Transf 44(5):1039–51
56. Javidi Sarafan M, Alizadeh R, Fattahi A, Valizadeh Ardalan M, Karimi N (2020) Heat and mass transfer and thermodynamic analysis of power-law fluid flow in a porous microchannel. J Therm Anal Calorim 141(5):2145–64
57. Li F, Ma Q, Xin G, Zhang J, Wang X (2020) Heat transfer and flow characteristics of microchannels with solid and porous ribs. Appl Therm Eng 178:115639
58. Dehghan M, Valipour MS, Saedodin S (2016) Microchannels enhanced by porous materials: Heat transfer enhancement or pressure drop increment? Energy Convers Manag 110:22–32
59. Dehghan M, Valipour MS, Saedodin S, Mahmoudi Y (2016) Investigation of forced convection through entrance region of a porous-filled microchannel: An analytical study based on the scale analysis. Appl Therm Eng 99:446–54
60. Haddad OM, Abuzaid MM, Al-Nimr MA (2005) Developing free-convection gas flow in a vertical open-ended microchannel filled with porous media. Numer Heat Transf Part A Appl 48(7):693–710
61. Jia YT, Xia GD, Zong LX, Ma DD, Tang YX (2018) A comparative study of experimental flow boiling heat transfer and pressure drop characteristics in porous-wall microchannel heat sink. Int J Heat Mass Transf 127:818–33
62. Mondal S, De S (2013) Mass transport in a porous microchannel for non-Newtonian fluid with electrokinetic effects. Electrophoresis. 34(5):668–73
63. Zargartalebi M, Azaiez J (2019) Flow dynamics and heat transfer in partially porous microchannel heat sinks. J Fluid Mech 875:1035–57
64. Deng D, Tang Y, Liang D, He H, Yang S (2014) Flow boiling characteristics in porous heat sink with reentrant microchannels. Int J Heat Mass Transf 70:463–77
65. Hung TC, Huang YX, Yan WM (2013) Thermal performance of porous microchannel heat sink: Effects of enlarging channel outlet. Int Commun Heat Mass Transf 48:86–92
66. Lu G, Zhao J, Lin L, Wang XD, Yan WM (2017) A new scheme for reducing pressure drop and thermal resistance simultaneously in microchannel heat sinks with wavy porous fins. Int J Heat Mass Transf 111:1071–8
67. Hung TC, Huang YX, Yan WM (2015) Design of Porous-Microchannel Heat Sinks with Different Porous Configurations. Int J Mater Mech Manuf 4(2):89–94
68. Bar-Cohen A (2013) Gen-3 thermal management technology: Role of microchannels and nanostructures in an embedded cooling paradigm. J Nanotechnol Eng Med 4(2):1–3
69. Ghosh DP, Sharma D, Mohanty D, Saha SK, Raj R (2019) Facile Fabrication of Nanostructured Microchannels for Flow Boiling Heat Transfer Enhancement. Heat Transf Eng 40(7):537–48
70. Nagayama G, Sibuya S, Kawagoe M, Tsuruta T (2007) Heat transfer enhancement at nanostructured surface in parallel-plate microchannel. In Challenges of Power Engineering and Environment: Proceedings of the International Conference on Power Engineering 999-1006. Springer Berlin Heidelberg
71. Alam T, Li W, Chang W, Yang F, Khan J, Li C (2018) A comparative study of flow boiling HFE-7100 in silicon nanowire and plainwall microchannels. Int J Heat Mass Transf 124:829–40
72. Yang F, Li W, Dai X, Li C (2016) Flow boiling heat transfer of HFE-7000 in nanowire-coated microchannels. Appl Therm Eng 93:260–8
73. Ding Y, Jia L, Zhang Y, An Z (2019) Investigation on R141b convective condensation in microchannel with low surface energy coating and hierarchical nanostructures surface. Appl Therm Eng 155(April):480–8
74. Sharma D, Ghosh DP, Saha SK, Raj R (2019) Thermohydraulic characterization of flow boiling in a nanostructured microchannel heat sink with vapor venting manifold. Int J Heat Mass Transf 130:1249–59
75. Hedau G, Dey P, Raj R, Saha SK (2020) Combined effect of inlet restrictor and nanostructure on two-phase flow performance of parallel microchannel heat sinks. Int J Therm Sci 153(March):106339
76. Hendricks TJ, Krishnan S, Choi C, Chang CH, Paul B (2010) Enhancement of pool-boiling heat transfer using nanostructured surfaces on aluminum and copper. Int J Heat Mass Transf 53(15–16):3357–65
77. Gao L, Lyu J, Bai M, Li Y, Gao D, Shi L (2021) The microchannel combined hydrophobic nanostructure for enhancing boiling heat transfer. Appl Therm Eng 194(May):116962
78. Yao Z, Lu YW, Kandlikar SG (2012) Pool boiling heat transfer enhancement through nanostructures on silicon microchannels. J Nanotechnol Eng Med 3(3):1–8
79. Wei X, Joshi Y, Patterson MK (2007) Experimental and numerical study of a stacked microchannel heat sink for liquid cooling of microelectronic devices. J Heat Transfer 129(10):1432–44
80. Qu W, Mudawar I (2002) Experimental and numerical study of pressure drop and heat transfer in a single-phase micro-channel heat sink. Int J Heat Mass Transf 45(12):2549–65
81. Chen C, Teng JT, Cheng CH, Jin S, Huang S, Liu C et al (2014) A study on fluid flow and heat transfer in rectangular microchannels with various longitudinal vortex generators. Int J Heat Mass Transf 69:203–14
82. Dey P, Saha SK (2021) Fluid flow and heat transfer in microchannel with porous bio-inspired roughness. Int J Therm Sci 161(December 2020):106729
83. Rimbault B, Nguyen CT, Galanis N (2014) Experimental investigation of CuO-water nanofluid flow and heat transfer inside a microchannel heat sink. Int J Therm Sci 84:275–92
84. Burns MGSGW (1989) The Calibration of Thermocouples and Thermocouple Materials. U.S. Department of Commerce, National Institute of Standards and Technology 188
85. Ho CJ, Wei LC, Li ZW (2010) An experimental investigation of forced convective cooling performance of a microchannel heat sink with Al2O3/water nanofluid. Appl Therm Eng 30(2–3):96–103
86. Hedau G, Dey P, Raj R, Saha SK (2020) Experimental and numerical investigation of the effect of number of parallel microchannels on flow boiling heat transfer. Int J Heat Mass Transf 158:119973
87. Dede EM, Liu Y (2013) Experimental and numerical investigation of a multi-pass branching microchannel heat sink. Appl Therm Eng 55(1–2):51–60
88. Kadam ST, Kumar R, Abiev R (2019) Performance augmentation of single-phase heat transfer in open-type microchannel heat sink. J Thermophys Heat Transf 33(2):416–24

89. Markal B, Aydin O, Avci M (2019) Effect of hydraulic diameter on flow boiling in rectangular microchannels. Heat Mass Transf und Stoffuebertragung. 55(4):1033–44
90. Yang D, Wang Y, Ding G, Jin Z, Zhao J, Wang G (2017) Numerical and experimental analysis of cooling performance of single-phase array microchannel heat sinks with different pin-fin configurations. Appl Therm Eng 112:1547–56
91. Peles Y, Koşar A, Mishra C, Kuo CJ, Schneider B (2005) Forced convective heat transfer across a pin fin micro heat sink. Int J Heat Mass Transf 48(17):3615–27
92. Derive closed-form analytical solutions to math and engineering problems [Internet]
93. Pavuluri S, Maes J, Doster F (2018) Spontaneous imbibition in a microchannel: analytical solution and assessment of volume of fluid formulations. Microfluid Nanofluidics 22(8):0
94. Sahu PK, Golia A, Sen AK (2012) Analytical, numerical and experimental investigations of mixing fluids in microchannel. Microsyst Technol 18(6):823–32
95. Dey P, Raj D, Saha SK (2021) A Numerical Study on Condensation Heat Transfer Characteristics of R134a in Microchannel Under Varying Gravity Conditions. Microgravity Sci Technol 33(3)
96. PD (2018) Introduction to Numerical Computing. J Appl Comput Math 07(04)
97. Abiev RS (2013) Bubbles velocity, Taylor circulation rate and mass transfer model for slug flow in milli- and microchannels. Chem Eng J 227:66–79
98. Bordbar A, Taassob A, Zarnaghsh A, Kamali R (2018) Slug flow in microchannels: Numerical simulation and applications. J Ind Eng Chem 62:26–39
99. Jang SP, Choi SUS (2006) Cooling performance of a microchannel heat sink with nanofluids. Appl Therm Eng 26(17–18):2457–63
100. Raja Kuppusamy N, Saidur R, Ghazali NNN, Mohammed HA (2014) Numerical study of thermal enhancement in micro channel heat sink with secondary flow. Int J Heat Mass Transf 78:216–23
101. Kuppusamy NR, Mohammed HA, Lim CW (2013) Numerical investigation of trapezoidal grooved microchannel heat sink using nanofluids. Thermochim Acta 573:39–56
102. Shen H, Xie G, Wang CC (2019) The numerical simulation with staggered alternation locations and multi-flow directions on the thermal performance of double-layer microchannel heat sinks. Appl Therm Eng 163(March):114332
103. Leng C, Wang XD, Wang TH, Yan WM (2015) Optimization of thermal resistance and bottom wall temperature uniformity for double-layered microchannel heat sink. Energy Convers Manag 93:141–50
104. Wu JM, Zhao JY, Tseng KJ (2014) Parametric study on the performance of double-layered microchannels heat sink. Energy Convers Manag 80:550–60
105. Xia G, Zhai Y, Cui Z (2013) Numerical investigation of thermal enhancement in a micro heat sink with fan-shaped reentrant cavities and internal ribs. Appl Therm Eng 58(1–2):52–60
106. Szczukiewicz S, Magnini M, Thome JR (2014) Proposed models, ongoing experiments, and latest numerical simulations of microchannel two-phase flow boiling. Int J Multiph Flow 59:84–101
107. Yang M, Li MT, Hua YC, Wang W, Cao BY (2020) Experimental study on single-phase hybrid microchannel cooling using HFE-7100 for liquid-cooled chips. Int J Heat Mass Transf 160:120230
108. Arie MA, Shooshtari AH, Dessiatoun SV, Al-Hajri E, Ohadi MM (2015) Numerical modeling and thermal optimization of a single-phase flow manifold-microchannel plate heat exchanger. Int J Heat Mass Transf 81:478–89
109. Chauhan A, Sammakia B, Ghose K, Refai-Ahmed G, Agonafer D (2010) Hot spot mitigation using single-phase microchannel cooling for microprocessors. 2010 12th IEEE Intersoc Conf Therm Thermomechanical Phenom Electron Syst ITherm
110. Dede EM (2014) Single-phase microchannel cold plate for hybrid vehicle electronics. Annu IEEE Semicond Therm Meas Manag Symp 118–24
111. Lin Y, Luo Y, Li W, Cao Y, Tao Z, Shih TIP (2021) Single-phase and Two-phase Flow and Heat Transfer in Microchannel Heat Sink with Various Manifold Arrangements. Int J Heat Mass Transf 171:121118
112. Saad K Oudah, Ruixian Fang, Amitav Tikadar, Karim Egab, Chen Li JAK (2017) Imece2017-71627 Transfer Performance in a Single-Phase Microchannel Heat Sink 1–8
113. Sahar AM, Özdemir MR, Fayyadh EM, Wissink J, Mahmoud MM, Karayiannis TG (2016) Single phase flow pressure drop and heat transfer in rectangular metallic microchannels. Appl Therm Eng 93:1324–36
114. Sahar AM, Wissink J, Mahmoud MM, Karayiannis TG, Ishak MSA (2017) Effect of hydraulic diameter and aspect ratio on single phase flow and heat transfer in a rectangular microchannel. Appl Therm Eng 115:793–814
115. Sharma CS, Tiwari MK, Michel B, Poulikakos D (2013) Thermofluidics and energetics of a manifold microchannel heat sink for electronics with recovered hot water as working fluid. Int J Heat Mass Transf 58(1–2):135–51
116. Shkarah AJ, Sulaiman MY Bin, Ayob MRBH, Togun H (2013) A 3D numerical study of heat transfer in a single-phase microchannel heat sink using graphene, aluminum and silicon as substrates. Int Commun Heat Mass Transf 48:108–15
117. Zhang HY, Pinjala D, Wong TN, Toh KC, Joshi YK (2005) Single-phase liquid cooled microchannel heat sink for electronic packages. Appl Therm Eng 25(10):1472–87
118. Radwan A, Ookawara S, Ahmed M (2018) Thermal management of concentrator photovoltaic systems using two-phase flow boiling in double-layer microchannel heat sinks. Appl Energy 2019(241):404–19
119. Pourfattah F, Arani AAA, Babaie MR, Nguyen HM, Asadi A (2019) On the thermal characteristics of a manifold microchannel heat sink subjected to nanofluid using two-phase flow simulation. Int J Heat Mass Transf 143:118518
120. Chinnov EA, Ron'shin FV, Kabov OA (2016) Two-phase flow patterns in short horizontal rectangular microchannels. Int J Multiph Flow 80:57–68
121. Cho SC, Wang Y (2014) Two-phase flow dynamics in a micro channel with heterogeneous surfaces. Int J Heat Mass Transf 71:349–60
122. Wang Y, Sefiane K, Wang ZG, Harmand S (2014) Analysis of two-phase pressure drop fluctuations during micro-channel flow boiling. Int J Heat Mass Transf 70:353–62
123. Keepaiboon C, Wongwises S (2015) Two-phase flow patterns and heat transfer characteristics of R134a refrigerant during flow boiling in a single rectangular micro-channel. Exp Therm Fluid Sci 66:36–45
124. Thiangtham P, Keepaiboon C, Kiatpachai P, Asirvatham LG, Mahian O, Dalkilic AS et al (2016) An experimental study on two-phase flow patterns and heat transfer characteristics during boiling of R134a flowing through a multi-microchannel heat sink. Int J Heat Mass Transf 98:390–400
125. Ali N, Teixeira JA, Addali A (2018) A Review on Nanofluids: Fabrication, Stability, and Thermophysical Properties. J Nanomater
126. Sarafraz MM, Yang B, Pourmehran O, Arjomandi M, Ghomashchi R (2019) Fluid and heat transfer characteristics of aqueous graphene nanoplatelet (GNP) nanofluid in a microchannel. Int Commun Heat Mass Transf 107(June):24–33
127. Arani AAA, Akbari OA, Safaei MR, Marzban A, Alrashed AAAA, Ahmadi GR et al (2017) Heat transfer improvement of water/single-wall carbon nanotubes (SWCNT) nanofluid in a novel design of a truncated double-layered microchannel heat sink. Int J Heat Mass Transf 113:780–95

128. Azizi Z, Alamdari A, Malayeri MR (2015) Convective heat transfer of Cu-water nanofluid in a cylindrical microchannel heat sink. Energy Convers Manag 101:515–24
129. Bahiraei M, Jamshidmofid M, Goodarzi M (2019) Efficacy of a hybrid nanofluid in a new microchannel heat sink equipped with both secondary channels and ribs. J Mol Liq 273:88–98
130. Hatami M, Ganji DD (2014) Thermal and flow analysis of microchannel heat sink (MCHS) cooled by Cu-water nanofluid using porous media approach and least square method. Energy Convers Manag 78:347–58
131. Hung TC, Yan WM (2012) Enhancement of thermal performance in double-layered microchannel heat sink with nanofluids. Int J Heat Mass Transf 55(11–12):3225–38
132. Al-Baghdadi MARS, Noor ZMH, Zeiny A, Burns A, Wen D (2020) CFD analysis of a nanofluid-based microchannel heat sink. Therm Sci Eng Prog 20(August):100685
133. Tokit EM, Mohammed HA, Yusoff MZ (2012) Thermal performance of optimized interrupted microchannel heat sink (IMCHS) using nanofluids. Int Commun Heat Mass Transf 39(10):1595–604
134. Vinoth R, Sachuthananthan B (2021) Flow and heat transfer behavior of hybrid nanofluid through microchannel with two different channels. Int Commun Heat Mass Transf 123:105194
135. Marathe A, Zhang Y, Blanks G, Kumbhare N, Abdulla G, Rountree B (2017) An empirical survey of performance and energy efficiency variation on Intel processors. Proc E2SC 2017 5th Int Work Energy Effic Supercomput - Held conjunction with SC 2017 Int Conf High Perform Comput Networking, Storage Anal
136. Liu S, Lin T, Luo X, Chen M, Jiang X (2006) A microjet array cooling system for thermal management of active radars and high-brightness LEDs. Proc - Electron Components Technol Conf 2006:1634–8
137. Browne MC, Norton B, McCormack SJ (2015) Phase change materials for photovoltaic thermal management. Renew Sustain Energy Rev 47:762–82
138. Jiang L, Mikkelsen J, Koo JM, Huber D, Yao S, Zhang L et al (2002) Closed-loop electroosmotic microchannel cooling system for VLSI circuits. IEEE Trans Components Packag Technol 25(3):347–55
139. Chen G, Jia M, Zhang S, Tang Y, Wan Z (2020) Pool boiling enhancement of novel interconnected microchannels with reentrant cavities for high-power electronics cooling. Int J Heat Mass Transf 156
140. Silvério V, Cardoso S, Gaspar J, Freitas PP, Moreira ALN (2015) Design, fabrication and test of an integrated multi-microchannel heat sink for electronics cooling. Sens Actuators A Phys 235:14–27
141. Bahiraei M, Heshmatian S (2017) Thermal performance and second law characteristics of two new microchannel heat sinks operated with hybrid nanofluid containing graphene-silver nanoparticles. Energy Convers Manag 2018(168):357–70
142. Hou F, Zhang H, Huang D, Fan J, Liu F, Lin T et al (2020) Microchannel Thermal Management System with Two-Phase Flow for Power Electronics over 500 W/cm2Heat Dissipation. IEEE Trans Power Electron 35(10):10592–600
143. Jaikumar A, Kandlikar SG (2015) Enhanced pool boiling for electronics cooling using porous fin tops on open microchannels with FC-87. Appl Therm Eng 91:426–33
144. Jung KW, Kharangate CR, Lee H, Palko J, Zhou F, Asheghi M et al (2017) Microchannel cooling strategies for high heat flux (1 kW/cm2) power electronic applications. Proc 16th Intersoc Conf Therm Thermomechanical Phenom Electron Syst ITherm 98–104
145. Laguna G, Azarkish H, Vilarrubí M, Ibañez M, Rosell J, Betancourt Y et al (2017) Microfluidic cell cooling system for electronics. THERMINIC 2017 - 23rd Int Work Therm Investig ICs Sys 1–4
146. Sakanova A, Yin S, Zhao J, Wu JM, Leong KC (2014) Optimization and comparison of double-layer and double-side micro-channel heat sinks with nanofluid for power electronics cooling. Appl Therm Eng 65(1–2):124–34
147. Sharma CS, Tiwari MK, Zimmermann S, Brunschwiler T, Schlottig G, Michel B et al (2015) Energy efficient hotspot-targeted embedded liquid cooling of electronics. Appl Energy 138:414–22
148. Redo MA, Jeong J, Giannetti N, Enoki K, Yamaguchi S, Saito K et al (2018) Characterization of two-phase flow distribution in microchannel heat exchanger header for air-conditioning system. Exp Therm Fluid Sci 2019(106):183–93
149. Pan M, Wang H, Zhong Y, Hu M, Zhou X, Dong G et al (2019) Experimental investigation of the heat transfer performance of microchannel heat exchangers with fan-shaped cavities. Int J Heat Mass Transf 134:1199–208
150. Hu Y, Yuill DP, Ebrahimifakhar A (2020) The effects of outdoor air-side fouling on frost growth and heat transfer characteristics of a microchannel heat exchanger: An experimental study. Int J Heat Mass Transf 151:119423
151. Mahvi AJ, Garimella S (2019) Two-phase flow distribution of saturated refrigerants in microchannel heat exchanger headers. Int J Refrig 104:84–94
152. Glazar V, Frankovic B, Trp A (2015) Experimental and numerical study of the compact heat exchanger with different microchannel shapes. Int J Refrig 51:144–53
153. Kwon B, Maniscalco NI, Jacobi AM, King WP (2018) High power density air-cooled microchannel heat exchanger. Int J Heat Mass Transf 118:1276–83
154. Li H, Hrnjak P (2015) An experimentally validated model for microchannel heat exchanger incorporating lubricant effect. Int J Refrig 59:259–68
155. Mazaheri N, Bahiraei M, Razi S (2021) Two-phase analysis of nanofluid flow within an innovative four-layer microchannel heat exchanger: Focusing on energy efficiency principle. Powder Technol 383:484–97
156. Mohammadian SK, Seyf HR, Zhang Y (2014) Performance augmentation and optimization of aluminum oxide-water nanofluid flow in a two-fluid microchannel heat exchanger. J Heat Transfer 136(2):1–9
157. Shi HN, Ma T, Chu W xiao, Wang Q (2017) Optimization of inlet part of a microchannel ceramic heat exchanger using surrogate model coupled with genetic algorithm. Energy Convers Manag 149:988–996
158. Yih J, Wang H (2020) Experimental characterization of thermal-hydraulic performance of a microchannel heat exchanger for waste heat recovery. Energy Convers Manag 204(September): 112309
159. Zhou F, Zhou W, Qiu Q, Yu W, Chu X (2018) Investigation of fluid flow and heat transfer characteristics of parallel flow double-layer microchannel heat exchanger. Appl Therm Eng 137:616–31
160. Zhou F, Zhou W, Zhang C, Qiu Q, Yuan D, Chu X (2020) Experimental and numerical studies on heat transfer enhancement of microchannel heat exchanger embedded with different shape micropillars. Appl Therm Eng 175(April):115296
161. Wei A, Ren X, Lin S, Zhang X (2020) CFD analysis on flow and heat transfer mechanism of a microchannel Ω-shape heat pipe under zero gravity condition. Int J Heat Mass Transf 163:120448
162. Diallo TMO, Yu M, Zhou J, Zhao X, Shittu S, Li G et al (2019) Energy performance analysis of a novel solar PVT loop heat pipe employing a microchannel heat pipe evaporator and a PCM triple heat exchanger. Energy 167:866–88
163. Modjinou M, Ji J, Yuan W, Zhou F, Holliday S, Waqas A et al (2019) Performance comparison of encapsulated PCM PV/T, microchannel heat pipe PV/T and conventional PV/T systems. Energy 166:1249–66
164. Li G, Zhang G, He W, Ji J, Lv S, Chen X et al (2016) Performance analysis on a solar concentrating thermoelectric generator

using the micro-channel heat pipe array. ENERGY Convers Manag 112:191–8
165. Li G, Ji J, Zhang G, He W, Chen X, Chen H (2016) Performance analysis on a novel micro-channel heat pipe evacuated tube solar collector-incorporated thermoelectric generation. Int J Energy Res. 40(15):2117–27
166. Shittu S, Li G, Zhao X, Zhou J, Ma X, Akhlaghi YG (2020) Experimental study and exergy analysis of photovoltaic-thermoelectric with flat plate micro-channel heat pipe. Energy Convers Manag 207(October 2019):112515
167. Song Z, Ji J, Cai J, Li Z, Han K (2021) Performance analyses on a novel heat pump with a hybrid condenser combined with flat plate micro-channel heat pipe plus TEG and FPV evaporator. Energy Convers Manag 228(October):113606
168. Ali AYM, Abo-Zahhad EM, Elqady HI, Rabie M, Elkady MF, El-Shazly AH (2020) Impact of microchannel heat sink configuration on the performance of high concentrator photovoltaic solar module. Energy Reports 6:260–5
169. Abo-Zahhad EM, Ookawara S, Esmail MFC, El-Shazly AH, Elkady MF, Radwan A (2020) Thermal management of high concentrator solar cell using new designs of stepwise varying width microchannel cooling scheme. Appl Therm Eng 172(July 2019):115124
170. Acharya N (2020) On the flow patterns and thermal behaviour of hybrid nanofluid flow inside a microchannel in presence of radiative solar energy. J Therm Anal Calorim 141(4):1425–42
171. Ahlatli S, Mare T, Estelle P, Doner N (2016) Thermal performance of carbon nanotube nanofluids in solar microchannel collectors: An experimental study. Int J Technol 7(2):219–26